JOURNAL OF GEOPHYSICAL RESEARCH, VOL. 92, NO. D11, PAGES 13,315–13,343, NOVEMBER 20, 1987

# A Doubled $CO_2$ Climate Sensitivity Experiment With a Global Climate Model Including a Simple Ocean

C. A. WILSON AND J. F. B. MITCHELL

*Meteorological Office, Bracknell, Berkshire, England*

The sensitivity of a global climate model to increased atmospheric $CO_2$ concentrations is presented, assessed, and compared with earlier studies. The ocean is represented by a 50-m slab in which the heat convergence due to oceanic dynamics is prescribed, producing an accurate simulation of sea surface temperatures, sea-ice extents, and associated features in the control simulation. Changes in surface temperature are qualitatively similar to those found in earlier studies using models with similar or lower horizontal resolution, although the global warming is slightly larger. The simulated changes in hydrology agree broadly with those in studies made with higher horizontal resolution and prescribed changes in sea surface temperatures and include a drying over the northern mid-latitude continents. Many of the discrepancies in the responses of different models can be traced to differences in the simulations of present-day climate. The choice of convective parametrization appears to influence the sensitivity of the simulated response in the tropics.

## 1. INTRODUCTION

Over the last 27 years, concentrations of atmospheric carbon dioxide levels have increased by 8%, and there is evidence that concentrations have risen by 15–30% since 1860 [*Reichle et al.*, 1985]. There is speculation that $CO_2$ levels could reach 550 ppm (about twice the estimated preindustrial level) by the end of the twenty-first century [*Trabalka et al.*, 1985]. Evidence from numerical models suggests that enhanced $CO_2$ concentrations would lead to significant changes in climate (see, for example, *Schlesinger and Mitchell* [1985]) with potential economic and human consequences.

The investigations of the sensitivity of climate to enhanced carbon dioxide concentrations have produced a variety of estimates of the magnitude and distribution of the expected response [*Schlesinger and Mitchell*, 1985]. The calculated global mean surface warming due to doubling carbon dioxide concentrations ranges from about 1.5° to 4.5°C, the higher values occurring in recent simulations with model-generated cloud [*Schlesinger and Mitchell*, 1985; *Wetherald and Manabe*, 1986]. Whereas there is some qualitative agreement amongst existing studies on the more detailed aspects of the response, including enhanced warming and precipitation in high latitudes in winter and a general reduction in upper tropospheric cloud, there are also marked disagreements. For example, *Washington and Meehl* [1984] report a general increase in soil moisture in northern and mid-latitudes in summer, whereas studies carried out by Manabe and colleagues [e.g. *Manabe and Wetherald*, 1986] and *Mitchell* [1986] suggest that decreases in soil moisture are more likely.

*Schlesinger and Mitchell* [1985] show large discrepancies in the simulation of present-day climate in three contemporary climate models from different institutions. The response of a model to small perturbations will depend strongly on the simulation of the unperturbed climate [*Spelman and Manabe, 1984; Palmer and Mansfield*, 1986; *Mitchell et al.* 1987]. Hence a necessary condition for the reliable numerical prediction of climate change is that the models' control simulation is realistic. Although current climate models exhibit various deficiencies, we believe that one should not postpone sensitivity studies until one has a perfect model. However, it is important that the shortcomings of the model used in such a study are documented, so that they may be taken into account when assessing the response to the imposed change.

Most studies to date have employed a simple representation of the ocean, calculating sea surface temperatures without allowing for oceanic heat transport. On the other hand, *Mitchell* [1983] and *Mitchell and Lupton* [1984] used an alternative method. Sea surface temperatures in the control simulation were specified from climatological data, thereby implicitly including the effects of oceanic advection. The changes in sea surface temperature in the anomaly (enhanced $CO_2$) simulations were then determined to an increasing degree of sophistication in a series of perturbation experiments, by assuming that for small perturbations the changes in surface heating are related linearly to the local changes in sea surface temperature. Whereas in the more usual approach, 10–20 years of simulation are required to bring the ocean and atmosphere to equilibrium, the atmosphere equilibrates within a year when the sea surface temperatures are prescribed. Hence Mitchell and his coworkers were able to use higher horizontal resolution than in other studies, without needing extra computing resources. However, with this approach there is no obvious method of estimating the changes in sea-ice extent, and in high latitudes, nonlocal effects become important [see *Mitchell and Lupton*, 1984].

*Hansen et al.* [1984] prescribed the oceanic heat convergence (and mixed layer depth) in a low-resolution study of the effect of changes in the solar constant and enhanced $CO_2$ concentrations. In this paper we describe results from an experiment in which atmospheric $CO_2$ concentration is doubled, using a climate model with higher horizontal and vertical resolution but also using a prescribed oceanic heat convergence. This follows naturally from earlier experiments carried out within the Meteorological Office: instead of prescribing sea surface temperatures, we prescribe the oceanic heat convergence. However, the present work does not attempt to allow for changes in oceanic heat convergence that might accompany an increase in atmospheric $CO_2$.

## 2. THE MODEL

The climate model used in the present study comprises an atmospheric general circulation model coupled to a 50-m oceanic mixed layer and an energy-balance sea-ice model.

Published in 1987 by the American Geophysical Union.

Paper number 7D0658.

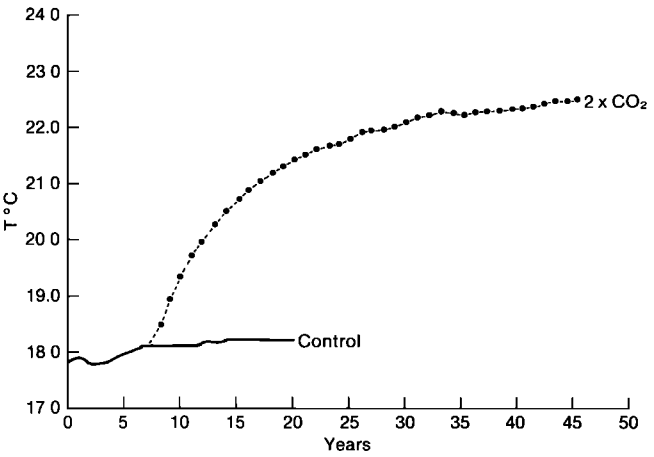


Fig. 1. Evolution of global mean annual mean slab ocean temperature (in degrees Celsius) for the control (solid line) and doubled $CO_2$ (dashed line) experiments.

The atmospheric model is the United Kingdom Meteorological Office model described by *Slingo* [1985], which has been used to investigate the impact of anomalies in sea surface temperature [*Palmer and Mansfield*, 1986], soil moisture [*Cunnington and Rowntree*, 1986], and the effect of increased atmospheric $CO_2$ [*Mitchell et al.*, 1987]. The primitive equations are solved using finite differences on 11 sigma ($\sigma$ = pressure/surface pressure) layers which are irregularly spaced, being concentrated near the boundary layer and the tropopause. A regular latitude-longitude grid is employed, computational stability and noise being controlled by a multipoint filter near the poles and by nonlinear diffusion. In this version the horizontal resolution has been degraded to 5° × 7.5° to allow longer simulations with the available computing resources, the time step has been increased to 20 min, and sea level pressure is filtered every 6 hours, using a 17-point Shapiro filter.

The treatment of the boundary layer uses the scheme of *Richards* [1980*a*, *b*], which is an extension of the ideas of *Clarke* [1970]. The boundary layer is allowed to occupy up to three of the lowest model layers, with the top being diagnosed at the position of the lowest inversion. In unstable conditions the turbulent mixing occurs through the lowest three layers, whilst in stable conditions the mixing is restricted to those layers below the diagnosed boundary layer top. The fluxes of heat, moisture, and momentum from the surface are based on Monin–Obukhov similarity theory [*Mitchell et al.* 1985], with evaporation limited, where appropriate, by soil moisture, following *Manabe* [1969]. Convection is modeled by a penetrative scheme [*Lyne and Rowntree*, 1976; *Rowntree*, 1984], which allows entrainment of environmental air and detrainment from the convective parcel at each level. In the original scheme, complete detrainment occurred in the final layer to which convection took place. This was modified to allow some detrainment to the layer above in order to represent the effect of penetration of an inversion by more buoyant plumes in a convective ensemble [A. Slingo, R. C. Wilderspin and R. N. B. Smith, The effect of improved physical parameterizations on simulations of cloudiness and the Earth's radiation budget in the tropics, in preparation, 1987]. This also provides a mechanism by which the boundary layer and free atmosphere can interact and improves the prediction of low cloud in the model by reducing the excessive low cloud over tropical oceans. Supersaturation produced either by large-scale ascent or following convection is removed by condensation to form precipitation. The convection scheme allows evaporation of the precipitation in the next layer below that in which it formed.

The seasonal and diurnal variations of solar radiation are represented, and radiative fluxes depend on temperature, the concentrations of water vapor, carbon dioxide and ozone, and on clouds. Long-wave fluxes are calculated using the emissivity approximation in a revised formulation by *Slingo and Wilderspin* [1986]. Over snow-free land the surface albedo is specified to vary geographically, with values derived from the global data on land cover and soils compiled by *Wilson and Henderson-Sellers* [1985]. Over snow-covered land, albedo increases with snow depth. Albedo is prescribed to be 0.06 over unfrozen sea and 0.7 over land ice. The radiation scheme has provision for three layer clouds (low, medium, and high) and a convective tower. The layer clouds are assumed to be one sigma layer thick, but convective cloud may occupy more than one sigma layer. The cloud reflectivity is specified as 0.2 for high cloud and 0.6 for other clouds. Clouds are assumed to be black for long-wave calculations, except for high cloud, which has an emissivity of 0.5.

The model was modified to include a cloud-prediction scheme for both convective and layer cloud, following *Slingo* [1980] and *Wilson and Mitchell* [1986]. Convective cloud amount is diagnosed from the maximum parcel size involved in moist convection and the base and top determined from the levels between which it occurs, whilst layer cloud amounts are simple functions of the layer relative humidities. In layers where convective cloud is diagnosed, the relative humidity of the layer free of convective cloud is used, assuming saturation in the convective cloud fraction. In the case of convection extending more than three layers, the cover in all but the lowest three layers is not allowed to exceed 8%, as a crude attempt to represent deep

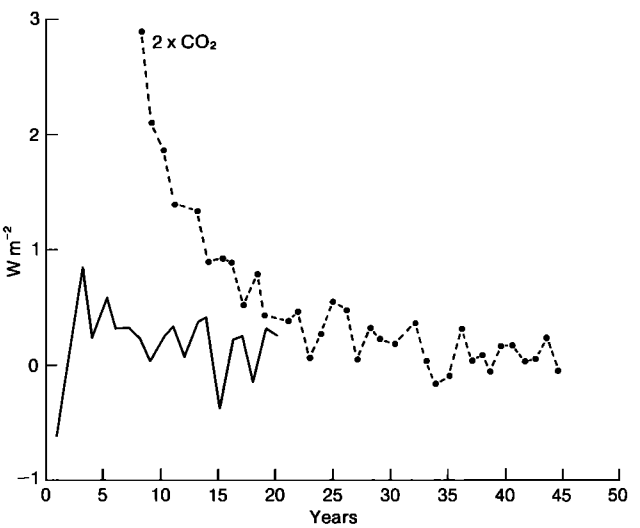


Fig. 2. Evolution of the global mean annual mean net heat flux into the slab ocean (in watts per square meter) for the control experiment (solid line) and the doubled $CO_2$ experiment (dashed line). This is calculated from the radiative, sensible and latent fluxes from the atmospheric model, the prescribed oceanic heat convergence and the heat required to melt snow falling into the sea, and multiplied by the fraction of the globe covered by sea, to give a mean net downward heat flux per total global area.

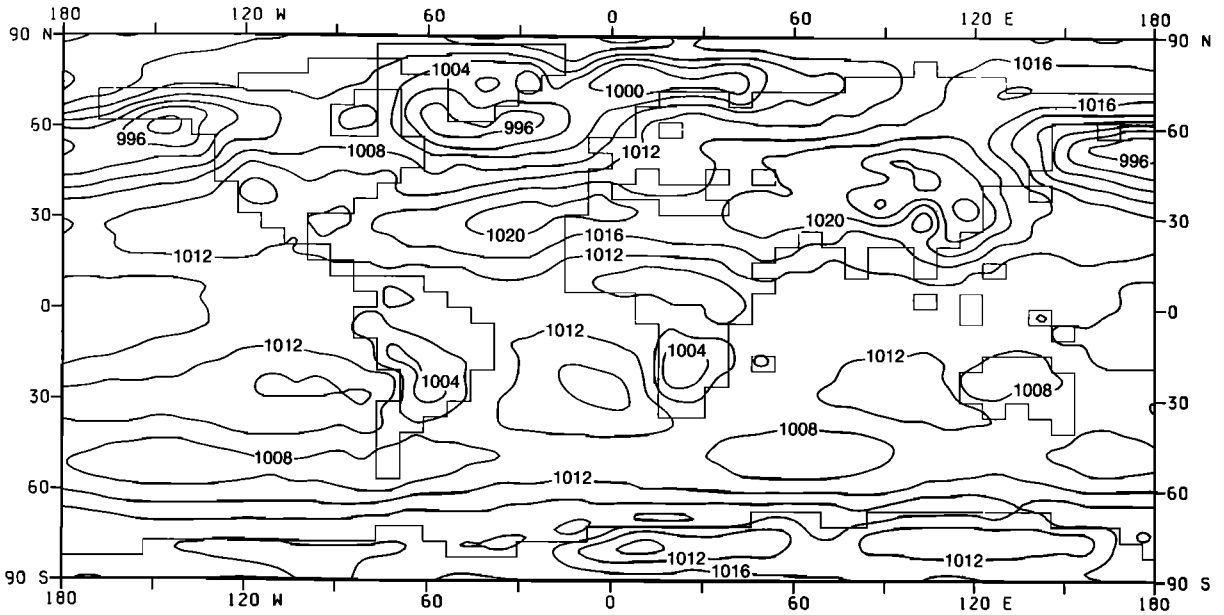


Fig. 3. Pressure reduced to mean sea level (*a*) for a mean of 15 northern winters (December–February, DJF) of the control experiment and (*b*) Observed (mean of three winters, 1983/1984 to 1985/1986, derived from Meteorological Office operational analyses, as shown by *Slingo and Pearson* [1987]). Contour interval is 4 mbar.

convective towers. Layer cloud may occur in any of the model layers except the top layer. Fractional cloud amount, $C$, is calculated from a simple quadratic function of relative humidity, $R$, if it exceeds a threshold value, $R_C$; i.e.,

$$C = (R-R_C)^2/(1-R_C)^2 \quad R>R_C$$

$$C = 0 \quad R \leq R_C$$

$R_C$ is 0.9, except for high clouds (the four layers next to the top) and for low cloud in the thin bottom layer next to the surface. For these, total cover is predicted if saturation is reached and zero otherwise. This restriction was imposed to limit the overprediction of high cloud found in tuning experiments. The low-cloud restriction is more physically reasonable, since the bottom layer is thinner and therefore unlikely to contain a cloud with radiative properties similar to those assumed until the depth-averaged humidity is close to saturation. The dependence of low cloud on low-level stability that was used in the original scheme [*Slingo, 1980*] was omitted, since the simulated cloud cover was reasonable without it.

The depth of the mixed layer (50 m) was chosen to be sufficient to allow for the seasonal storage of heat in the ocean [*Meehl and Washington*, 1985] without unduly prolonging the

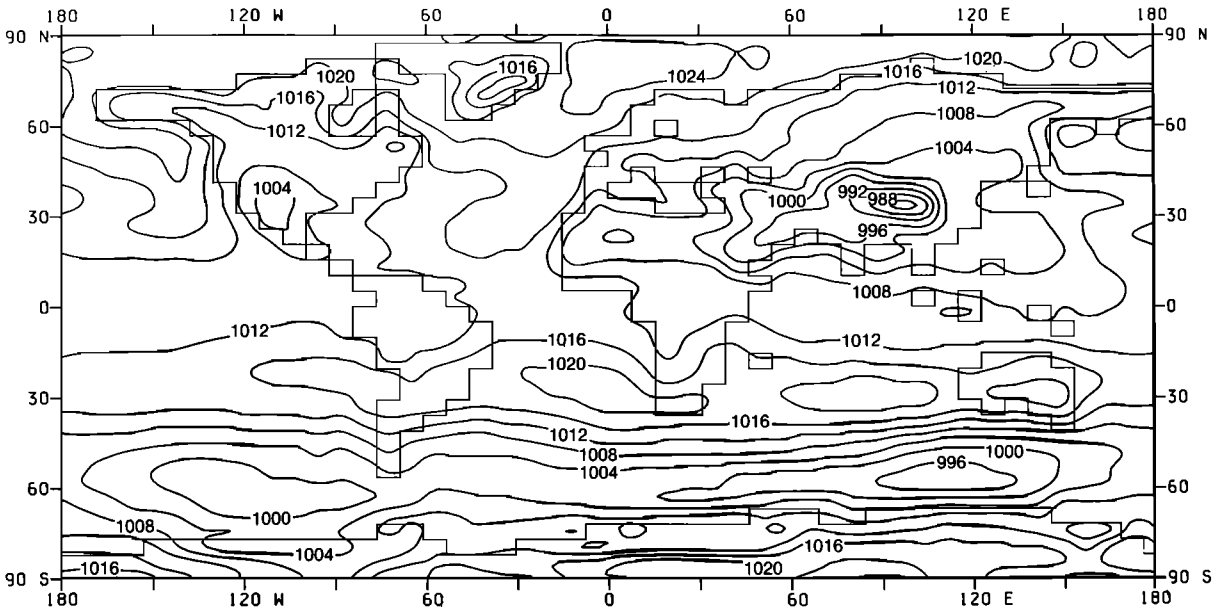


Fig. 4*a*

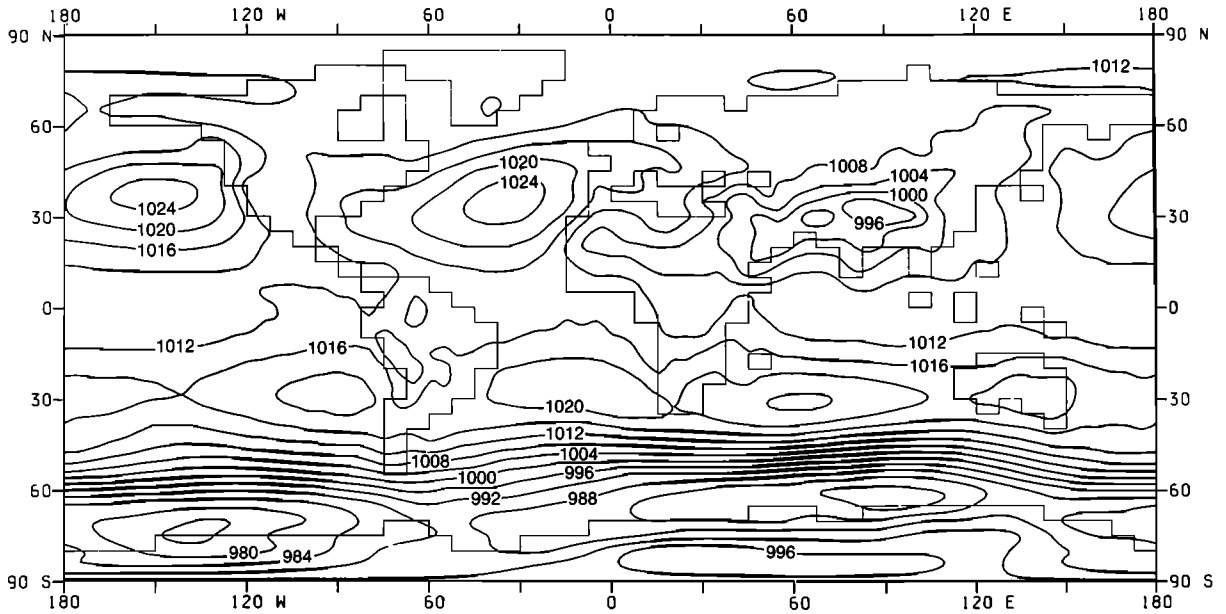


Fig. 4*b*

Fig. 4. Pressure reduced to mean sea level (*a*) for a mean of 15 northern summers (June–August, JJA) of the control experiment and (*b*) for an observed mean of three summers (1983 to 1985) derived from Meteorological Office operational analyses. Contour interval is 4 mbar.

thermal response time of the ocean. The evolution of the mixed layer temperature $T$ at each point is given by

$$\rho h c_p \frac{dT}{dt} = S + C \qquad (1)$$

where $\rho$ and $c_p$ are the density and specific heat of seawater, respectively, $h$ is the depth, $S$ is the heat flux through the surface, and $C$ is the prescribed heat convergence due to oceanic processes (advection, convection, etc). An effective $C$ for the model was determined by diagnosing $S$ in a 4-year atmospheric simulation in which the seasonal variation of sea surface temperatures (and so $dT/dt$) were prescribed from climatology and solving (1) for $C$ as a function of time and space. In the coupled model, sea surface temperatures are updated every 5 days, based on the net surface heating from the atmosphere and the specified heat convergence.

Sea ice forms when the ocean temperature falls below the freezing point of seawater, 271.2 K. The surface temperature of sea ice is updated every atmospheric model time step so that the effect of the diurnal cycle on both the short and long wave radiation budgets is included [*Gordon and Bottomley*, 1984]. Surface albedo increases linearly from 0.4 at 271.2 K to the land ice value of 0.7 at or below 261.2 K. The decrease in albedo as the temperature increases is intended to represent the presence of melt ponds and inhomogeneous cover over a grid square as the melting point is approached, since there is no provision for fractional ice cover of a grid square. Snowfall on top of ice and the diffusive heat flux through the ice are also included. Ice and

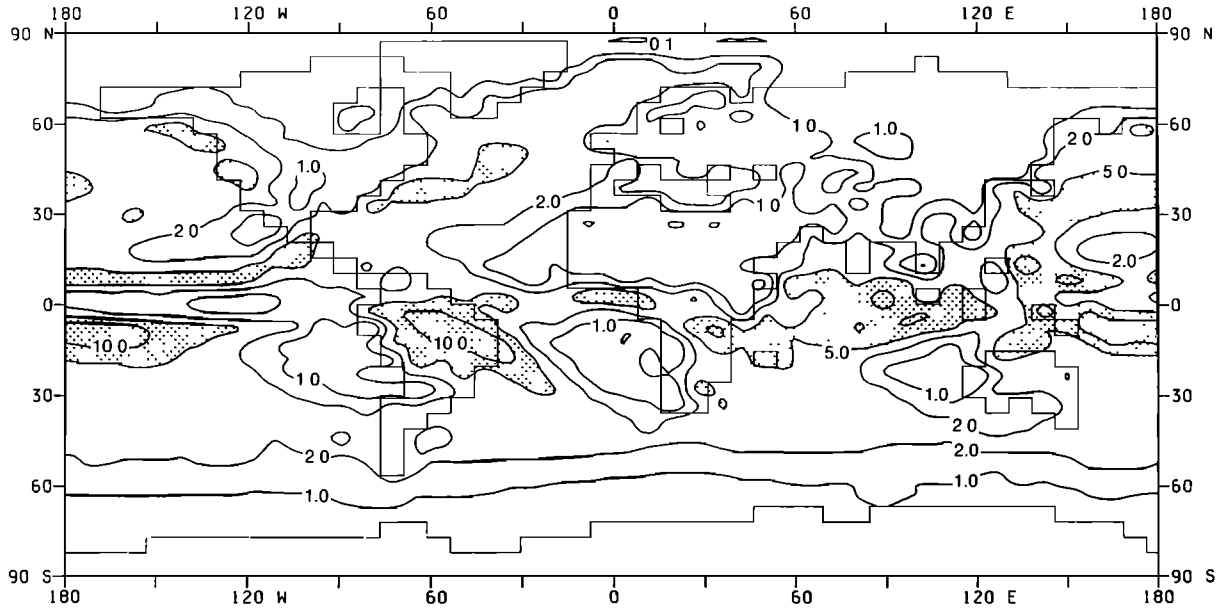


Fig. 5*a*

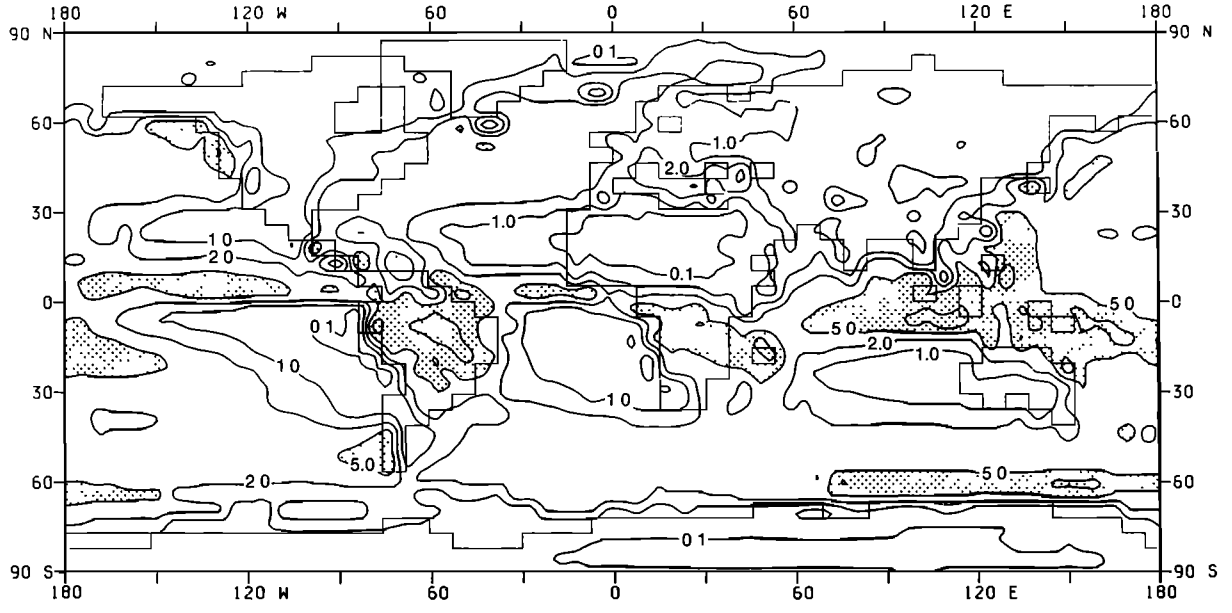


Fig. 5*b*

Fig. 5. Precipitation in northern winter (DJF) (*a*) from a 15-year mean of the control experiment and (*b*) from the climatology of *Jaeger* [1976]. Contours at 0.1, 1, 2, 5, 10, 20, and 40 mm $day^{-1}$, shaded above 5 mm $day^{-1}$.

snow depths and changes in classification are only updated every 5 days, using the accumulated heat budgets and snowfall, which simplifies coding and adequately represents the growth and decay of ice [*Gordon and Bottomley*, 1984]. The temperature of the mixed layer under the ice is kept at freezing point. (If there is ice at a point which was ice-free in the prescribed SST integration, the specified heat convergence is either used to reduce the thickness of ice, if positive, or if negative, is redistributed evenly over the ice-free points of the hemisphere).

The albedo formulation for sea ice is similar to that proposed by *Robock* [1980] and allows ice to melt more easily than would a discontinuous large jump of albedo at the melting point. With increased $CO_2$ relatively greater ice melt might be expected to occur, using a gradual as opposed to a discontinuous change in albedo with temperature and hence a discontinuous sensitivity for the global surface temperature increase, as shown by *Washington and Meehl* [1986]. A disadvantage of our scheme is that the albedo could be seriously underestimated if there is significant snowfall on the ice (M. Bottomley, personal communication, 1985).

## 3. The Experiments

The control integration simulated 20 complete years, and at the end of year 7, the anomaly integration was started with an instantaneous doubling of $CO_2$ amount and ran for 38 years.

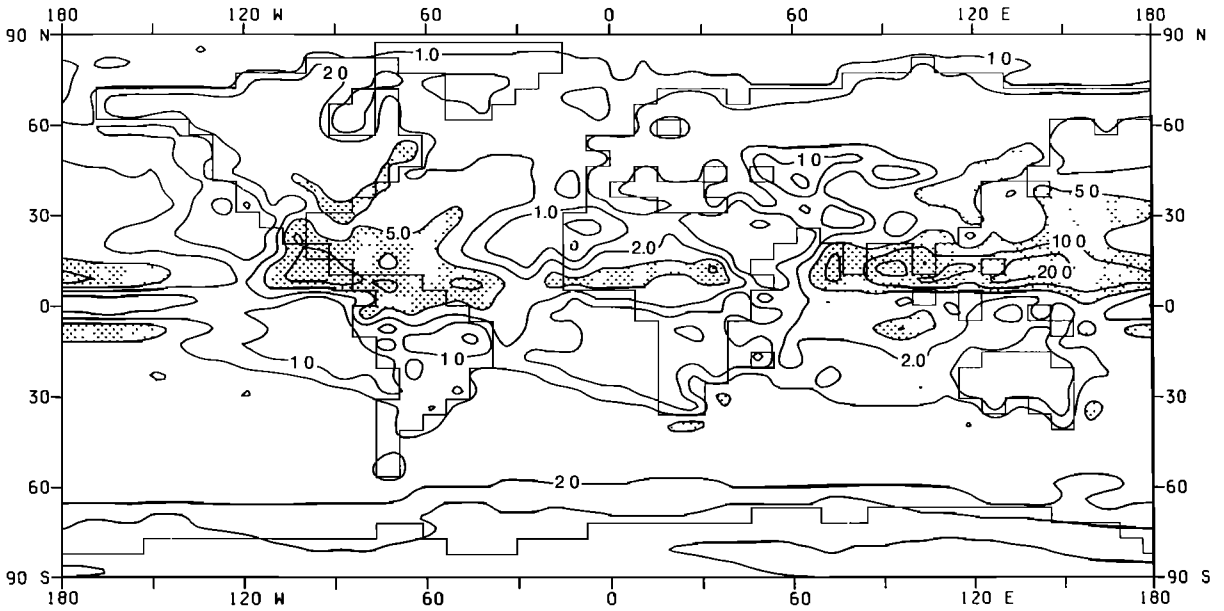


Fig. 6*a*

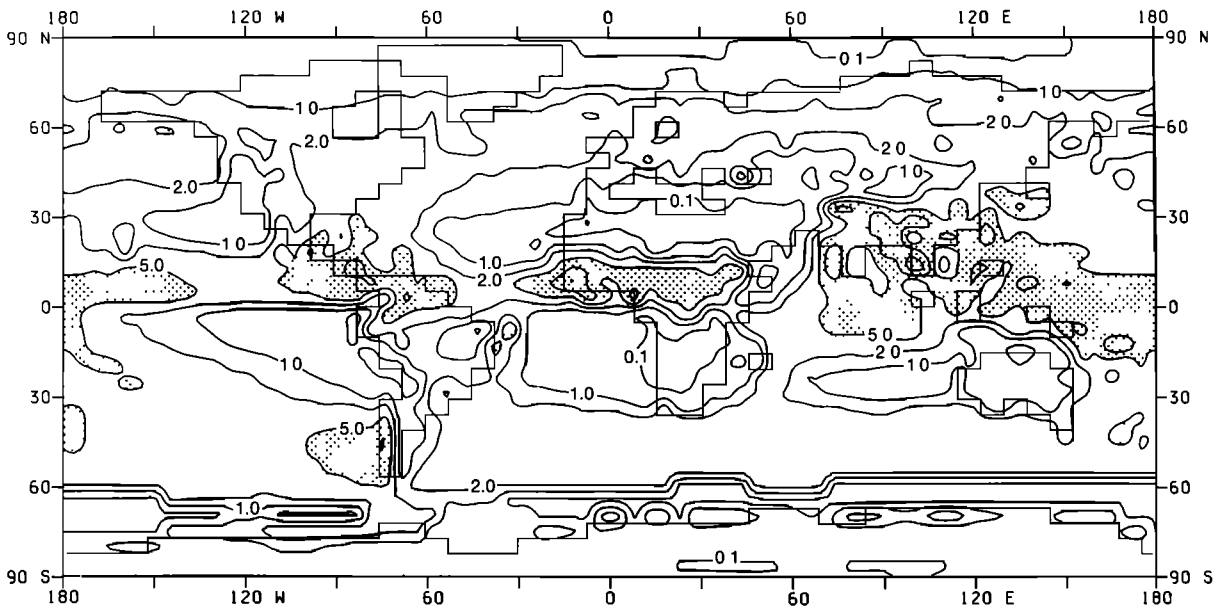


Fig. 6*b*

Fig. 6. As in Figure 5, but for JJA.

The time dependence of the global mean sea temperature (Figure 1) and the net heat flux into the mixed layer (Figure 2) show that whilst the control experiment has reached an approximate equilibrium after 10 years, the anomaly has not yet fully attained its equilibrium after 25 years. Nevertheless, the net heating is only of order 1/4 W m$^{-2}$ and the year-to-year temperature change is markedly less rapid than the early response. The temperature curve closely follows the exponential law

$$\Delta T(t) = \Delta T_{eq}\,[1 - \exp(-\tfrac{t}{\tau})]$$

with $\Delta T_{eq}$ for the slab ocean being about ~4.5°C and $\tau$ ~9 years, so that by year 25 over 90% of the eventual equilibrium change has been obtained. Also, the major differences in circulation and simulation are consistent and similar for the last 15 years of the experiment, for which results are presented later.

The initial net heat flux into the surface $H_0$ in the anomaly integration is ~3 W m$^{-2}$ and the difference in net radiation balance at the top of the atmosphere (not shown) is essentially the same. If the model were to adjust to equilibrium like a radiative blackbody, the heat capacity of 50 m of water would imply an e-folding time of ~2 years (the response time is $\tau = \rho c_p \Delta T / H_0$ where $\rho$ and $c_p$ are the density and specific heat of seawater, respectively, and $\Delta T$ ~1.1 K is the equilibrium

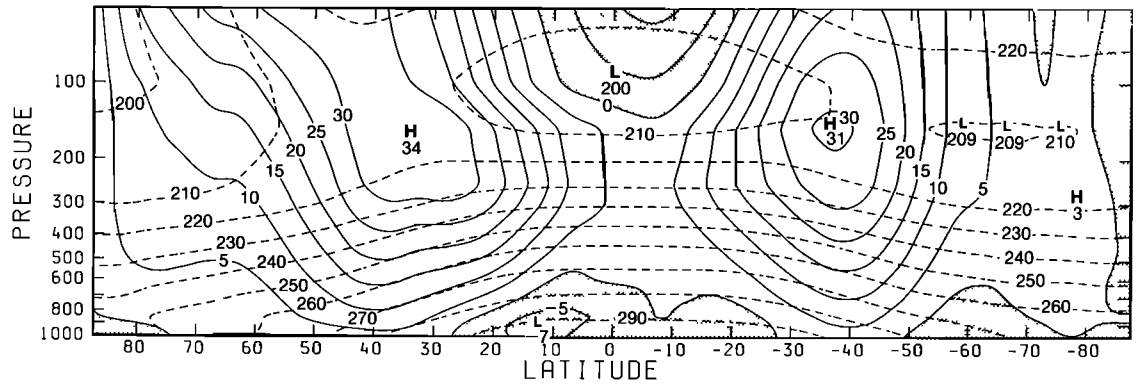


Fig. 7*a*

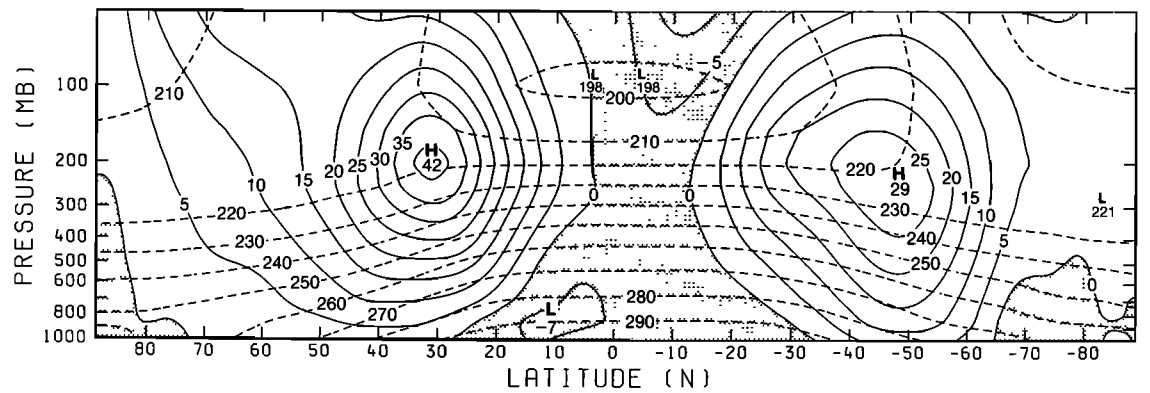


Fig. 7*b*

Fig. 7. As in Figure 3, but for zonally averaged zonal winds (full lines, meters per second) and temperatures (dashed lines, degrees Kelvin) as a function of log (pressure). Easterly (negative) winds shaded. Contour intervals are 5 m $s^{-1}$ and 10 K.

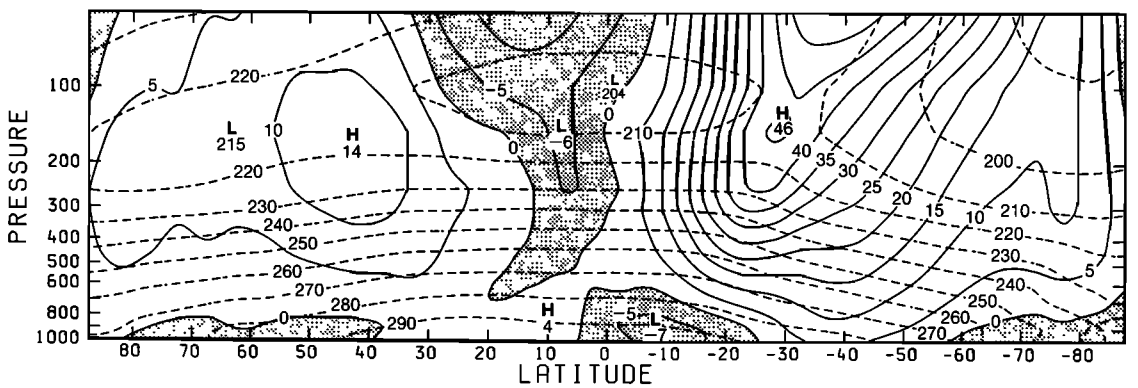


Fig. 8*a*

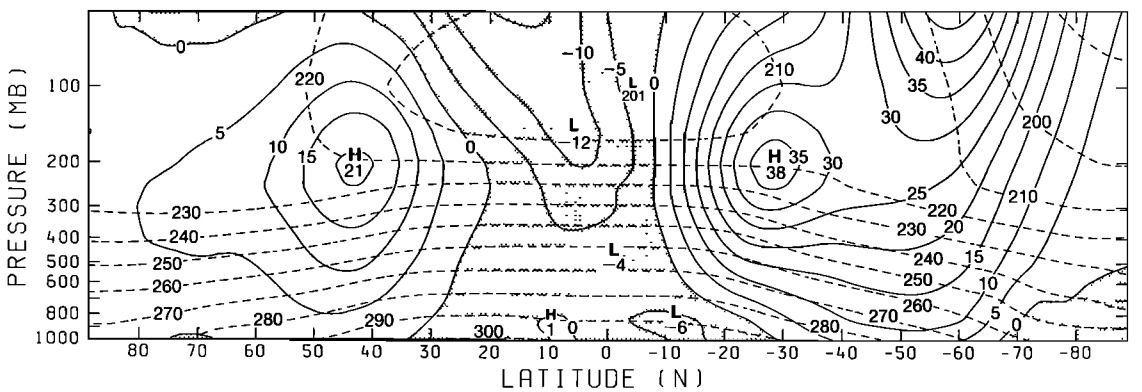


Fig. 8*b*

Fig. 8. As in Figure 7, but for JJA.

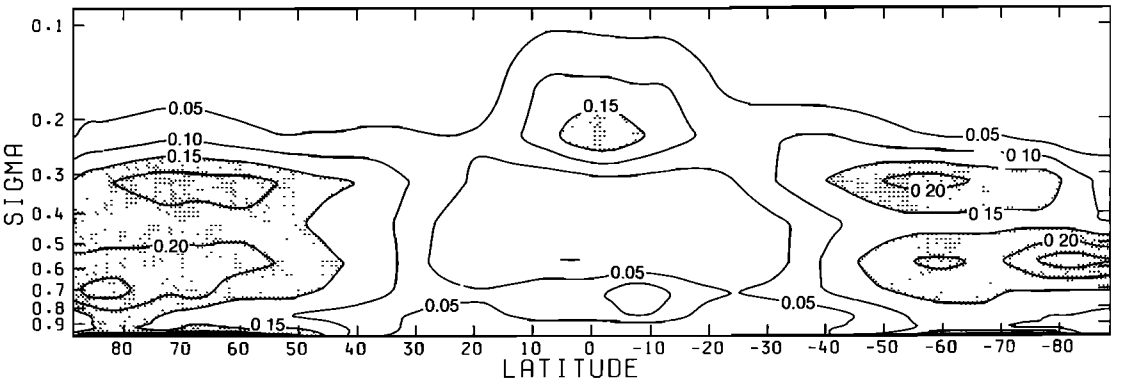


Fig. 9*a*

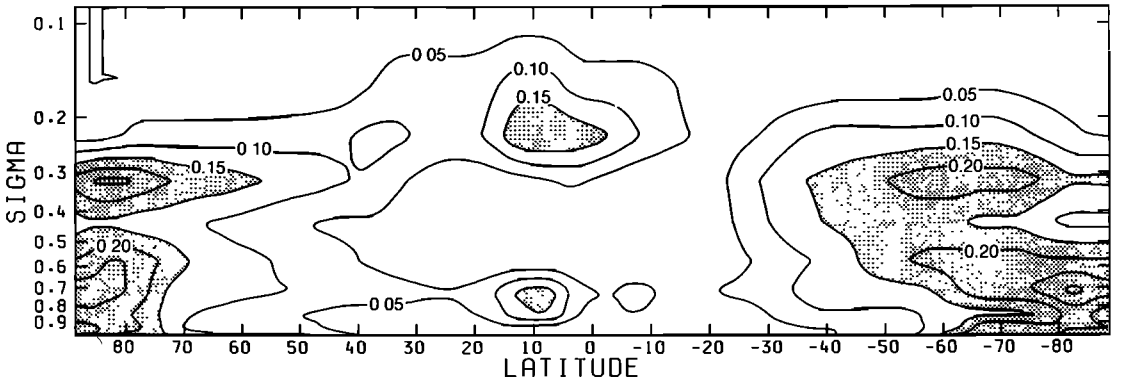


Fig. 9*b*

Fig. 9. (*a*) Log(sigma)-latitude cross section of zonal-mean layer cloud cover meaned over 15 northern winters (DJF) of the control experiment. Contour interval is 5% of total cover, stippled above 15%. (*b*) As in Figure 9a, but for a mean of 15 northern summers (JJA).

temperature change in the absence of feedbacks). As noted by *Hansen et al.* [1984] feedbacks which magnify the eventual temperature increase also prolong the approach to equilibrium by a similar factor; this is also found here.

## 4. The Control Simulation of Observed Climate

As noted in section 1, any climate model used to simulate climate change should produce a reasonable simulation of the present climate, and the shortcomings of the model should be documented. Therefore the behavior of the coupled model used here with the present level of $CO_2$ is briefly described, and its ability to simulate the present climate and especially its seasonal variation is evaluated. Charts for the means of December, January, and February (DJF) and June, July, and August (JJA), averaged over the last 15 years of the control integration, will mostly be shown, although results from other seasons will be mentioned where appropriate.

The mean sea level pressure for DJF (Figure 3*a*) reproduces fairly well the observed pattern (Figure 3*b*) in the northern hemisphere. The Siberian and Rockies highs are too weak and displaced southward and the Aleutian low extends too far over Alaska, but the general pattern is reasonable. In the southern hemisphere the most obvious error is the too shallow circumpolar trough (by about 15–20 mbar) positioned about 15° too far north. In JJA (Figure 4*a*) the southern depression belt is again about 12 mbar too shallow and is displaced to the north of the observed position (Figure 4*b*). In the northern hemisphere the subtropical highs over the Atlantic and Pacific Oceans are only weakly reproduced; pressure is too high over the pole, with a ridge toward the Azores high tending to give easterly flow over Western Europe. The heat lows over the American and Asian continents are reasonably well simulated, but there is erroneously low pressure over the northwest tropical Pacific.

Comparison of the precipitation of DJF (Figure 5*a*) with the observed data of *Jaeger* [1976] (Figure 5*b*) shows that the main convergence zones are reproduced but the drier areas of the subtropical oceans are wetter than observed. At higher latitudes, especially over the northern hemisphere continents, the agreement between the computed and observed amounts is quite close. In JJA (Figure 6*a*) the rainfall maxima of the Intertropical Convergence Zone (ITCZ) are near the observed positions but tend to be excessive over the oceans, especially the western Pacific and Bay of Bengal. Again, both the oceanic subtropics and most areas of north Africa are less dry than observed. Both the Indian and west African monsoons are weaker than observed, whilst the eastern coastal regions of northern continents are too wet.

The zonal mean model temperatures for DJF (Figure 7*a*) are generally similar to the observed (Figure 7*b*); the overall pattern is quite well simulated, and temperatures are generally within 5°C of observed. The low-level inversion at high latitudes in the northern hemisphere is simulated well; however, the tropical tropopause is too warm. The model temperatures for JJA (Figure 8*a*) are again in reasonable agreement with observed (Figure 8*b*), except that the tropical tropopause is again too

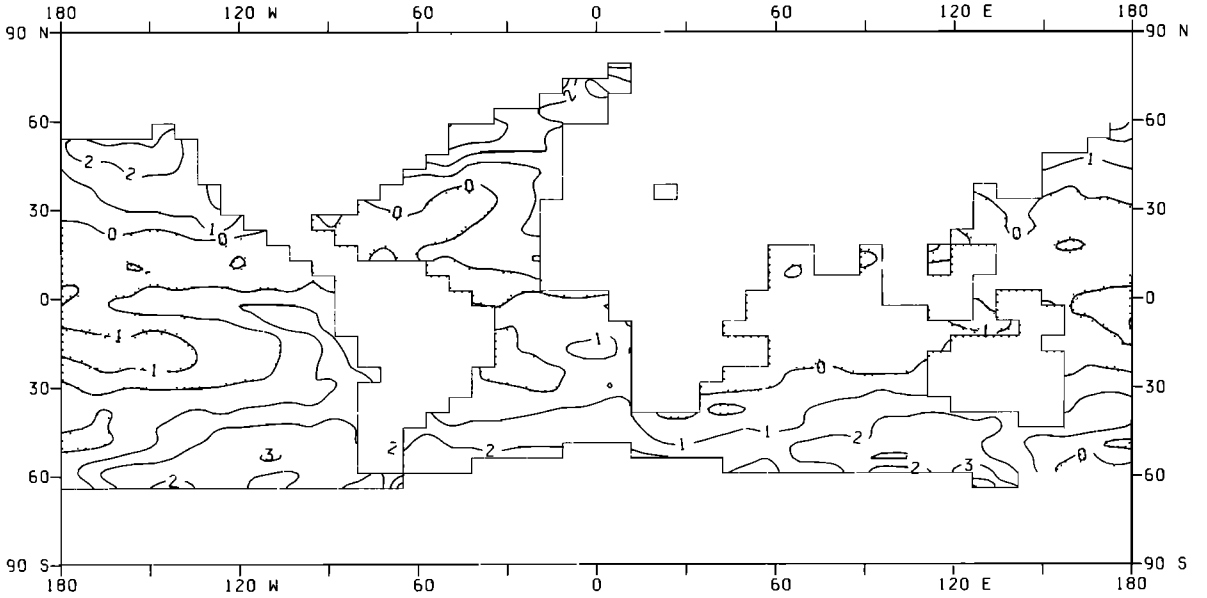


Fig. 10*a*

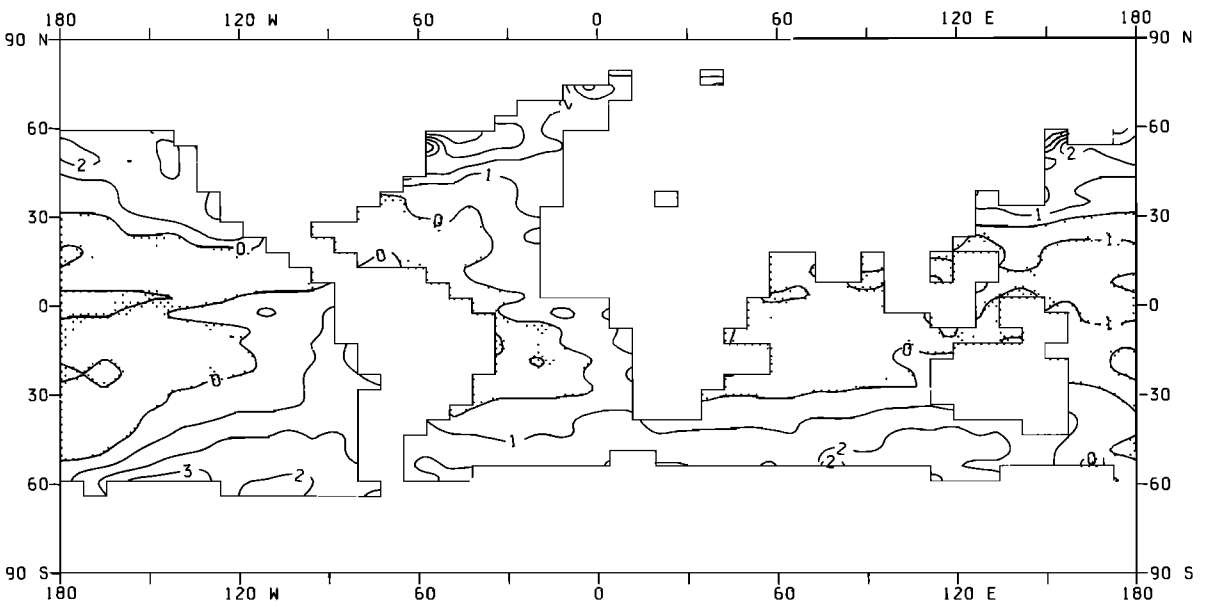


Fig. 10*b*

Fig. 10. Differences of sea surface temperatures simulated by the control experiment from those prescribed from observations for the experiment from which the heat convergence was calculated, meaned over 15 seasons (*a*) DJF. (*b*) JJA. Contour interval is 1 K, negative values (cooling) are stippled.

warm and upper tropospheric temperatures at high latitudes in the summer hemisphere are 10°–15°C too low. This is also true in the southern hemisphere in DJF.

The variation with height and latitude of the zonal mean westerly wind for DJF (Figure 7*a*) and JJA (Figure 8*a*) is quite similar to the observed (Figures 7*b* and 8*b*), with the main features being reproduced. The strength of the southern hemisphere jet in DJF is in excellent agreement, although it is positioned about 10° too far north and rather higher than observed. The northern hemisphere jet is about 10 m $s^{-1}$ too weak in both summer and winter, and in winter it does not show the observed separation from the stratospheric jet. This is also true in the southern hemisphere in winter, but given the model's resolution with only two layers above 100 mbar, it is not too surprising. This failure to separate the jets is also evident in the higher horizontal resolution version of the atmospheric model, as discussed by *Slingo and Pearson* [1987]. At low latitudes the observed easterlies are well simulated. However, there is a lack of stratospheric summer easterlies, and the low-level westerlies of the southern hemisphere are deficient; this is consistent with the shallow circumpolar trough noted earlier. The erroneous low-level easterly flow at northern hemisphere mid-latitudes in JJA reflects the deficiency in circulation noted previously in the discussion of the pressure pattern. Despite these deficiences the overall pattern is reasonably good, given the model's horizontal and vertical resolution.

The height-latitude diagrams of mean layer cloud amounts (convective amounts omitted) simulated by the model in the

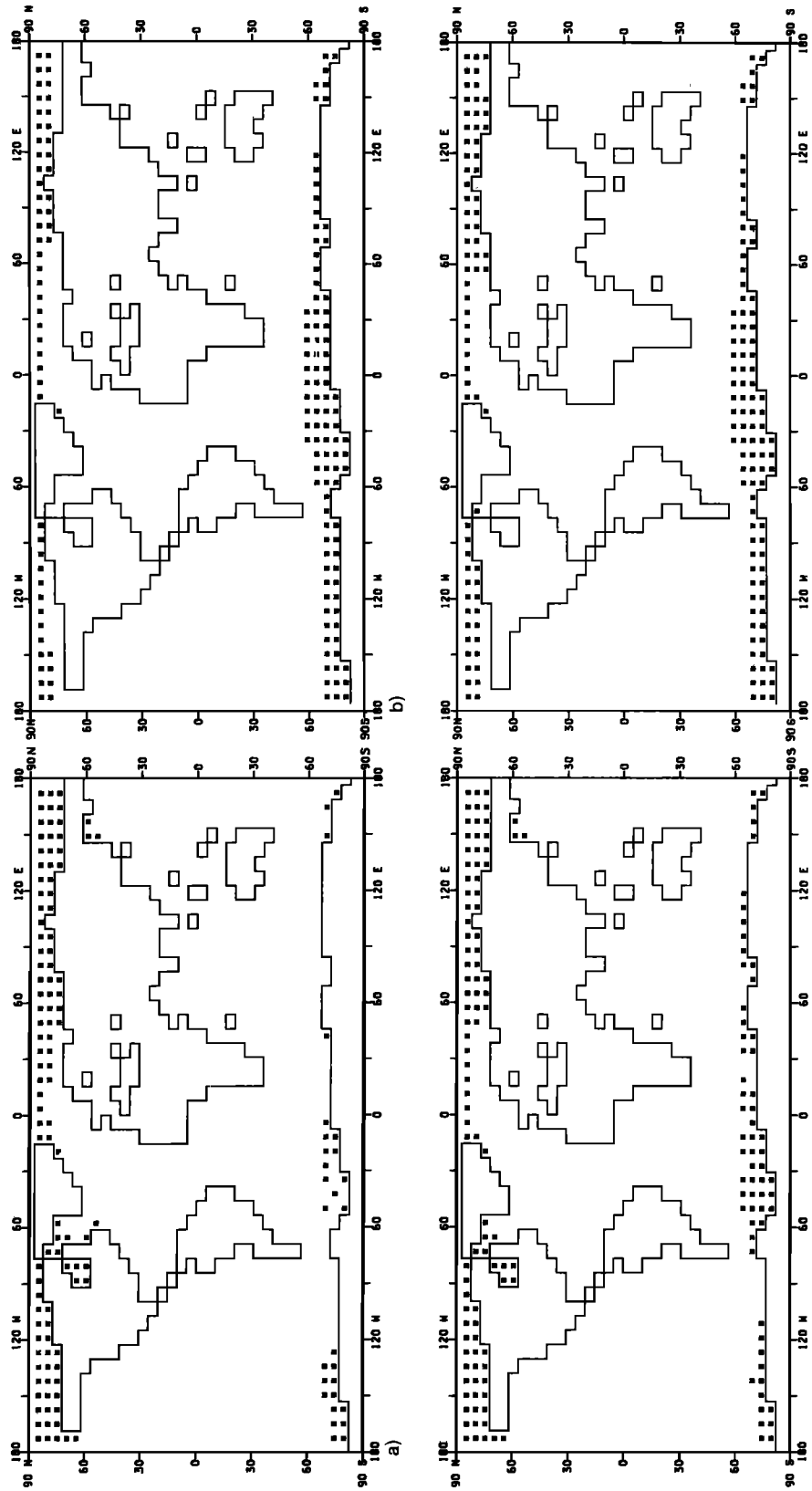


Fig. 11. Mean sea-ice extents in the control experiment for (*a*) February, (*b*) May, (*c*) August, and (*d*) November. A point is counted as sea ice in the mean if it was sea ice for more than half of the time during the 15 months meaned.

TABLE 1. Mean Sea-Ice Cover as a Fraction of Global Area or Area Between Specified Latitudes

| Experiment | Period | Globe | 90°N–30°N | 90°S–30°S |
|---|---|---|---|---|
| Prescribed sea-ice and SST for derivation of heat convergence | annual | 0.046 | 0.081 | 0.101 |
| | DJF | 0.040 | 0.101 | 0.057 |
| | MAM | 0.040 | 0.098 | 0.060 |
| | JJA | 0.051 | 0.064 | 0.135 |
| | SON | 0.053 | 0.059 | 0.151 |
| Control | annual | 0.045 | 0.076 | 0.102 |
| | DJF | 0.043 | 0.095 | 0.075 |
| | MAM | 0.039 | 0.100 | 0.055 |
| | JJA | 0.048 | 0.061 | 0.127 |
| | SON | 0.050 | 0.047 | 0.149 |
| Anomaly $2\times CO_2$ | annual | 0.019 | 0.042 | 0.032 |
| | DJF | 0.018 | 0.056 | 0.014 |
| | MAM | 0.022 | 0.077 | 0.007 |
| | JJA | 0.016 | 0.027 | 0.037 |
| | SON | 0.019 | 0.008 | 0.067 |

control experiment (Figure 9) show a number of realistic features. Observed estimates of cloud distribution are beset by a number of problems [*Crane and Barry*, 1984]. We use *Washington and Meehl*'s [1984] estimates of zonal clouds, derived from the data of *London* [1957] and *Sasamori et al.* [1972], as a rough guide to the actual cloud distributions in order to evaluate the model's distribution. The high-cloud maxima associated with the precipitation zones of the tropics and mid-latitudes are simulated well, as are the low cloud in the tropical convergence zone and the small-cloud amounts throughout most of the midtroposphere in the tropics and subtropics. There is too little low cloud generally, particularly near 60°N in JJA and 60°S in DJF; however, there are appreciable amounts of shallow convective cloud in these regions which are not shown by these diagrams. The excessive low cloud in the northern hemisphere winter at high latitudes occurs in the thin lowest model layer; this is a consequence of the boundary layer collapsing to one layer over the cold land surface and becoming saturated. In summary, the model-generated cloud amounts generally agree well with the observed estimates, and the major patterns are reproduced.

The differences of computed sea surface temperatures from those specified from observations in the integration used to derive the heat convergence have general similarities for both DJF (Figure 10*a*) and JJA (Figure 10*b*). Outside the tropics, sea surface temperatures are generally greater than observed, and most areas of the tropics are cooler than observed by 1°C or less. The obvious exceptions to this pattern are the eastern tropical oceans which are too warm by up to 1°C. This may be due to a coding error which was present in the convection scheme during the estimation of the heat convergence but which was corrected for the coupled simulations. Differences in net heating can also arise from changes in sea-ice extents, cloud, and circulation.

The sea-ice cover and its seasonal variation are an important influence on temperatures and low cloud at high latitudes. The reduction in sea ice in the anomaly experiment is also an important factor in determining the size of the eventual equilibrium warming due to doubled $CO_2$. Therefore it is important that the sea-ice simulation in the control integration is close to observations. Comparison of the mean extents for February, May, August, and November (Figure 11) for the model with observations from *Alexander and Mobley* [1976] show that a good seasonal variation has been obtained. The agreement in the northern hemisphere is especially good with the growth and decay of ice in Hudson Bay, to the east and west of Greenland and in the Sea of Okhotsk reproduced by the model. The mean depths of perennial ice in the Arctic are around 2 m, which also agree well with observations [*Maykut and Untersteiner*, 1971]. The Antarctic sea ice is also well modeled, though there is a very slight tendency for too large an extent in winter and autumn, particularly in the Ross Sea area. However, the removal of all but the perennial ice in the Ross and Weddell Seas in summer is successfully simulated. The fractional cover for both hemispheres is generally within a few percent of that specified from observations in the experiment to determine the oceanic heat convergence (Table 1).

The zonally averaged radiation budget (Figure 12) agrees reasonably well with the observations of *Stephens et al.* [1981]. The emitted flux generally agrees within 5–10 W $m^{-2}$, except at the north pole in winter, where it is 20 W $m^{-2}$ lower; the size of the equatorial dip is quite well captured, although absolute values are a little too high. Albedo agrees very well, except at the poles, where it is lower than observed estimates (which generally exceed 70%). This is to be expected with maximum albedos in the model for clouds of 60% and ice of 70%. Consequently, the net radiation is fairly well simulated, except in polar regions.

In summary, the model simulation of the observed climate with the present level of atmospheric $CO_2$ (323 parts per million by volume (ppmv)) is fairly good despite the deficiencies noted earlier. A major strength is the use of a specified oceanic heat convergence, which has resulted in a realistic variation of sea-ice and sea surface temperatures within a degree of observation over most of the ocean; this is a significant improvement on models which do not take oceanic heat transport into account. The model here has reproduced most of the main features of the observed temperature and precipitation, and in broad terms the model simulation of present climate is at least as good as, and often better than, that of other models used to study the effects of enhanced $CO_2$.

## 5. Model Response to Doubled $CO_2$

### 5.1 *Global Annual Mean*

We now consider the equilibrium climate obtained with double the present level of atmospheric $CO_2$ ($2\times 323$ ppmv).

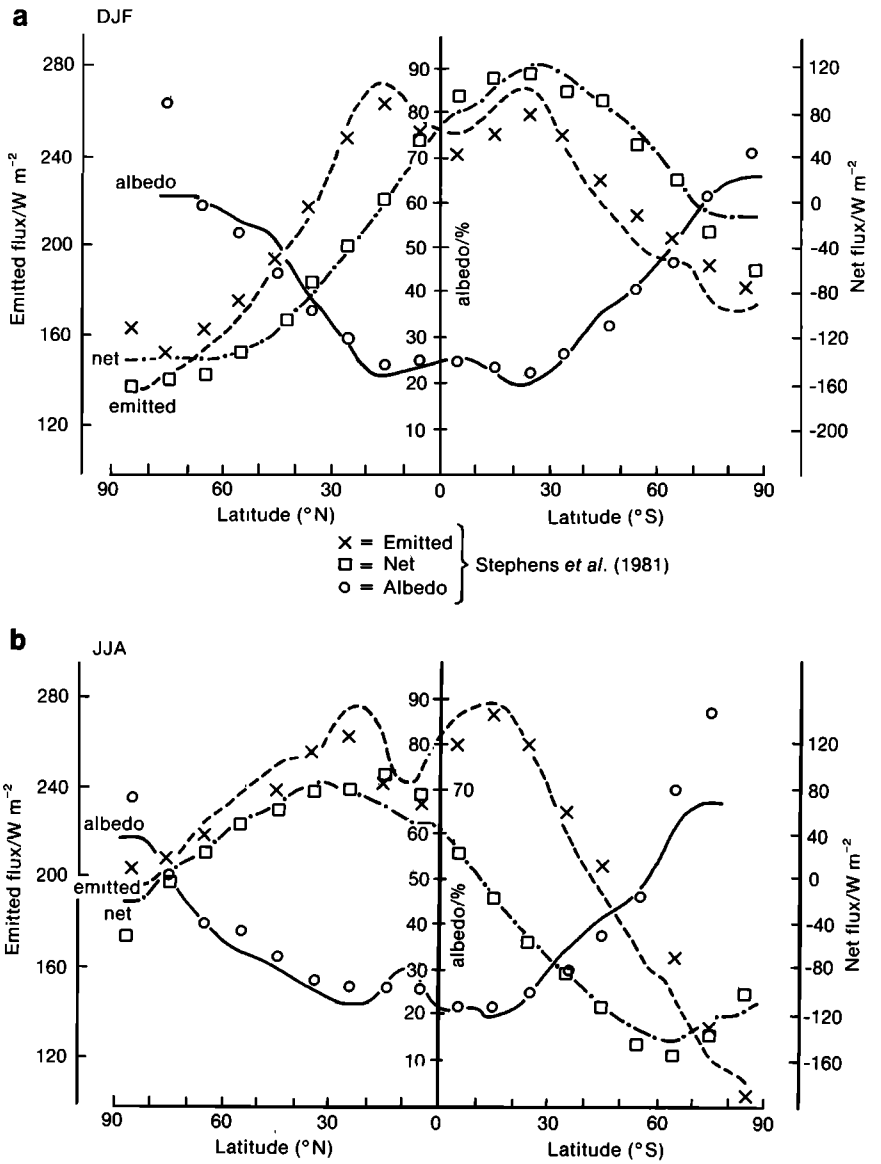


Fig. 12. Zonal means of infrared radiation emitted at the top of the atmosphere (in watts per square meter), net downward radiation at the top of the atmosphere (in watts per square meter), and planetary albedo (in percent) for a 15-year mean of the control experiment and from observations of *Stephens et al.* [1981]. (*a*) DJF. (*b*) JJA.

Unless otherwise stated, results are taken from the means of the last 15 years of the anomaly and control experiments.

The annual mean global average changes are given in Table 2. Sea surface temperature is warmer by 4.1°C, and the global surface temperature increase is 5.2°C. Evaporation and precipitation increase by 15%, whilst the total atmospheric moisture content increases by 41%. Cloud amount decreases by 4% (of total cover), mostly at medium and high levels, but there is more cloud above $\sigma = 0.23$. The troposphere warms by 5.7°C and the land surface by 6.4°C. The mean surface warming of 5.2°C is slightly larger than that found in similar experiments with climate models incorporating a simple mixed layer ocean performed elsewhere. *Hansen et al.* [1984] obtained global increases of surface air temperature of 4.2° and 4.8°C with sea-ice cover in the control simulation smaller and larger, respectively, than observed. *Washington and Meehl* [1984] obtained a warming of 3.5°C with overextensive sea ice in the control, and *Wetherald and Manabe* [1986] found a warming of 4.0°C. Possible reasons for the warming being greater in the present experiment are discussed later.

### 5.2 *Zonal Mean Changes*

The zonal mean temperature differences for DJF and JJA, averaged over the last 15 years of control and anomaly experiments (Figures 13*a* and 13*b*) show that the top layers of the model atmosphere cool by up to 6°C as a result of increased radiative cooling to space. The troposphere warms with temperature increases mostly greater than 4°C, except at low latitudes near the surface where they are of order 3.5°C. In the annual mean the largest increases of 7° to 8°C are in the upper tropical troposphere and are consistent with the tendency of the model's moist processes to adjust the vertical profile toward the moist adiabatic lapse rate; this lapse rate becomes smaller with increasing temperature and so amplifies temperature changes

TABLE 2. Changes Due to Doubled $CO_2$ (Global 15 year Means)

| | Change |
|---|---|
| Surface temperature, °C | |
| All Points | 5.2 |
| Sea* | 4.1 |
| Land | 6.4 |
| Tropospheric temperature,† °C | 5.7 |
| Atmospheric moisture content, % | 41 |
| Evaporation, % | 15 |
| Precipitation, % | 15 |
| Cloud cover, % | −4 |

* The sea temperature change does not include sea-ice points.
† The troposphere is taken as the first eight levels of the model up to $\sigma = 0.23$

with height. The maximum upper tropospheric warming extends into the summer hemisphere and decreases in altitude. Both this and the large warming of the lower atmosphere and surface at high latitudes in winter are qualitatively similar to the results of Wetherald and Manabe (reported by *Schlesinger and Mitchell* [1985]), though the changes at low latitudes are bigger here.

The vertical enhancement of temperature increases in the tropics is similar to that found by *Hansen et al.* [1984] who also used a penetrative convection scheme. *Wetherald and Manabe* [1986] and *Washington and Meehl* [1984] employed a moist convective adjustment procedure, which gave a less pronounced amplification [see *Mitchell et al.* 1985; *Schlesinger and Mitchell*, 1985]. The warming in the tropics is slightly larger than that found by *Hansen et al.* [1984], perhaps because their model is unable to represent an increase in (high) cloud above $\sigma = 0.103$. In our model the increase in high cloud (see Figure 16 for the zonal cloud changes below) reduces long-wave emission to space, while the compensating increase in the reflection of solar radiation is small because of the low albedo of high cloud. Part of the reason for the greater warming in the tropics compared to that found by Wetherald and Manabe is probably the greater reduction in tropospheric cloud. This may again be due to use of a penetrative convection scheme rather than moist convective adjustment as similar cloud reductions are also evident in the model used by *Hansen et al.* [1984].

At high latitudes the largest temperature increases are at the surface and in the lower atmosphere of the winter hemisphere. The stable profile results in this large warming being mainly confined to the lower atmosphere. The maximum changes near the surface, 12°C north of 70° N in DJF and near 65° S in JJA, are due to temperature albedo feedback and changes in sea ice. The melting of snow over land due to increased warming decreases the albedo, which leads to more warming, further melting of snow, and so on. The contribution to the surface warming of reductions in both thickness and extent of sea ice are discussed in section 5.3. Here we note that additional warming of the winter lower atmosphere arises from the removal of sea ice and the resulting enhanced fluxes of both sensible heat and moisture at high latitudes and possibly through increased convective and layer clouds, particularly high cloud (see Figure 16). The increased cloud has little effect on the solar

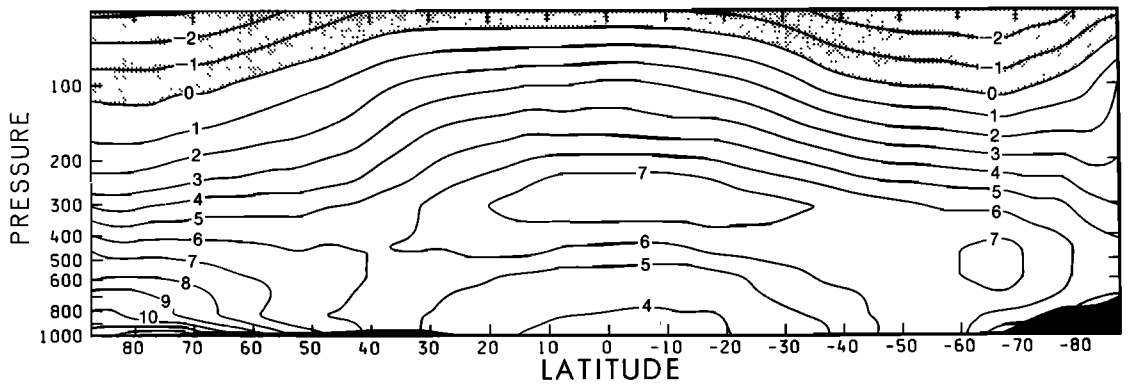


Fig. 13*a*

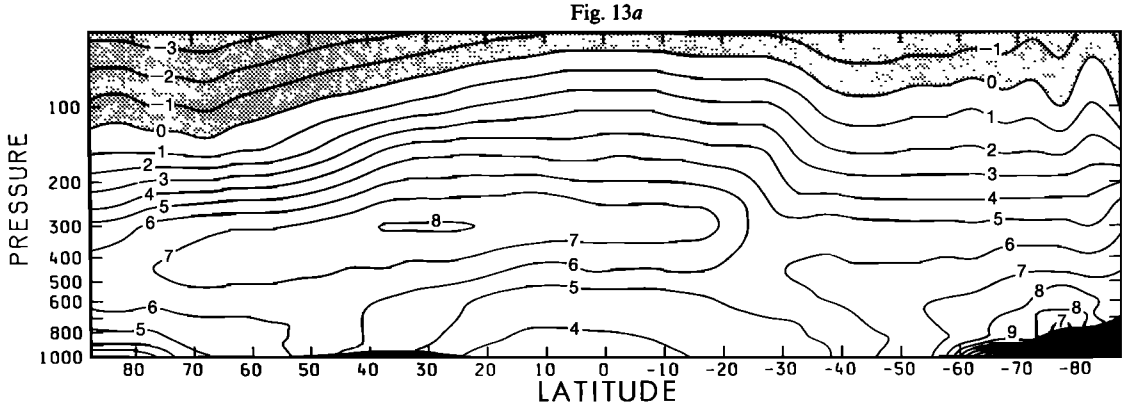


Fig. 13*b*

Fig. 13. Log(pressure)-latitude cross sections of difference of zonal-mean temperature ($2 \times CO_2$ − control, 15-year means), for (*a*) DJF and (*b*) JJA. Negative anomalies are stippled; contour interval is 1 K.

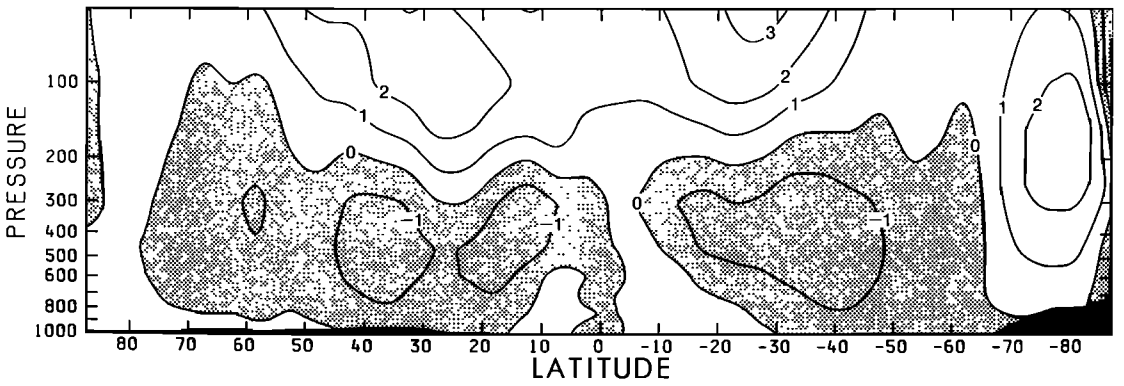


Fig. 14*a*

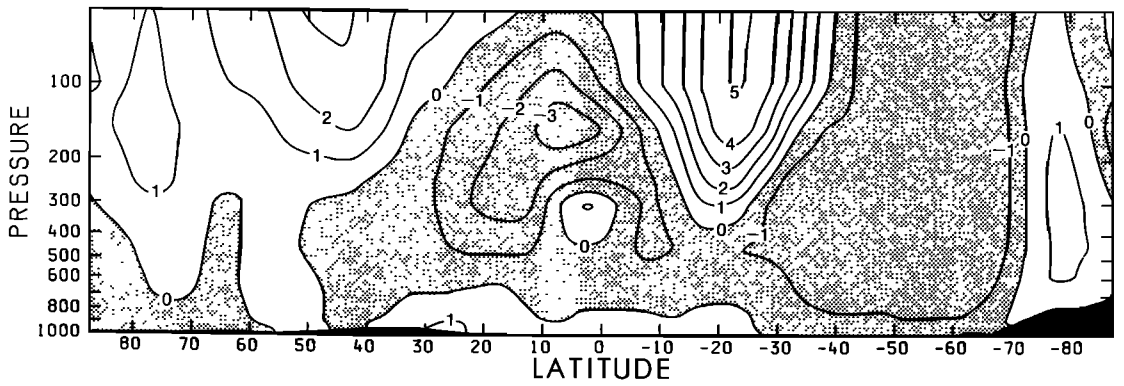


Fig. 14*b*

Fig. 14. As in Figure 16, but for westerly wind, with contour interval of 1 m $s^{-1}$.

beam, since the insolation is weak, but its influence on the long-wave radiation will tend to warm the atmosphere by reducing emission to space.

The changes in zonally averaged west to east wind (Figure 14) show stronger westerly flow at upper levels, with the strongest increase in low latitudes (though there is a decrease in the northern hemisphere centered around 200 mbar here in summer). The changes are largely to be expected, given the increased meridional temperature gradient (Figure 13) and assuming geostrophic balance, with the implied changes in geopotential gradients. The decrease in meridional gradient through much of the troposphere outside low latitudes results in generally weaker westerly flow. There is increased westerly flow south of 70° S in both seasons and at low altitudes north of 45° N in winter. There is an increasing reduction in westerly flow with height near 60° S at the latitudes where sea ice is removed during the control winter, as found in the sea-ice anomaly experiment of *Mitchell and Hills* [1986]. The changes, especially the increased westerly flow at upper levels, are generally smaller than those found in the experiments with prescribed sea surface temperature increases and doubled $CO_2$ with both prescribed cloud [*Mitchell et al.*, 1987] and model-generated cloud [*Mitchell et al.*, 1986].

As noted earlier global precipitation increases by 15%. The zonally averaged precipitation (Figure 15) increases almost everywhere except in the tropics of the winter hemisphere where rainfall is a minimum. The largest increases are in the main regions of convergence, i.e., the equatorial trough and in middle and high latitudes. The increases at all latitudes are generally much larger than those found in the enhanced $CO_2$ integrations performed at the Meteorological Office using prescribed sea surface temperatures [*Mitchell et al.*, 1987]. This might be expected, given the global surface temperature increase of 4°C over sea and 6°C over land and the consequent increase of atmospheric moisture by 41%, whereas *Mitchell et al.* [1987] prescribed sea surface temperature increases of 2°C, land temperature rose by 3°C, and the atmospheric moisture content increased by 20%. This is also shown by the much smaller zones of decrease or little change in precipitation in the present experiment compared to the previous experiments. However, the changes in precipitation are less determined by moisture content than by energy balance constraints (see *Mitchell et al.* [1987]).

The changes in zonal mean layer cloud (Figure 16) with doubled $CO_2$ show that there is a general decrease in middle-level clouds, increased high-level cloud at all latitudes, and some increases in low clouds at high latitudes. This pattern is similar to those found in studies at other institutes [see *Wetherald and Manabe*, 1986], and to the response in the higher-resolution model with a uniform 2 K increase in sea surface temperatures and $2 \times CO_2$ [*Mitchell et al.*, 1986].

The general reduction in tropospheric cloud is particularly marked in the main precipitation zones of the tropics and mid-latitudes (cf. Figure 15) where there are large increases in precipitation. The greater moisture content of the atmosphere and deeper convection contribute to the increased precipitation, whilst the raising of the tropopause, increased convection, and greater vertical motion into the lower stratosphere lead to a decrease in area-mean relative humidity and cloud amount [*Mitchell et al.*, 1986]. The cloud reductions are generally greater than those found by *Wetherald and Manabe* [1986] and *Washington and Meehl* [1984] but are similar to the results of

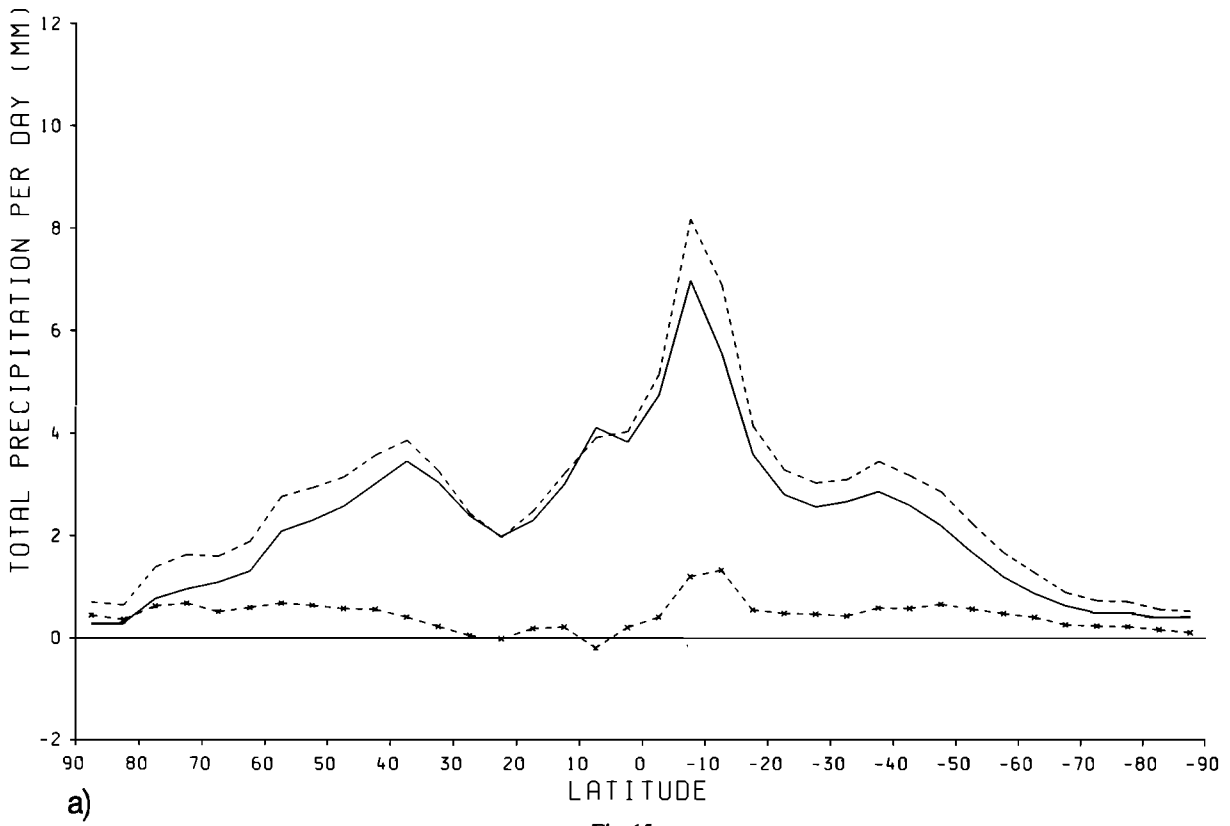


Fig. 15*a*

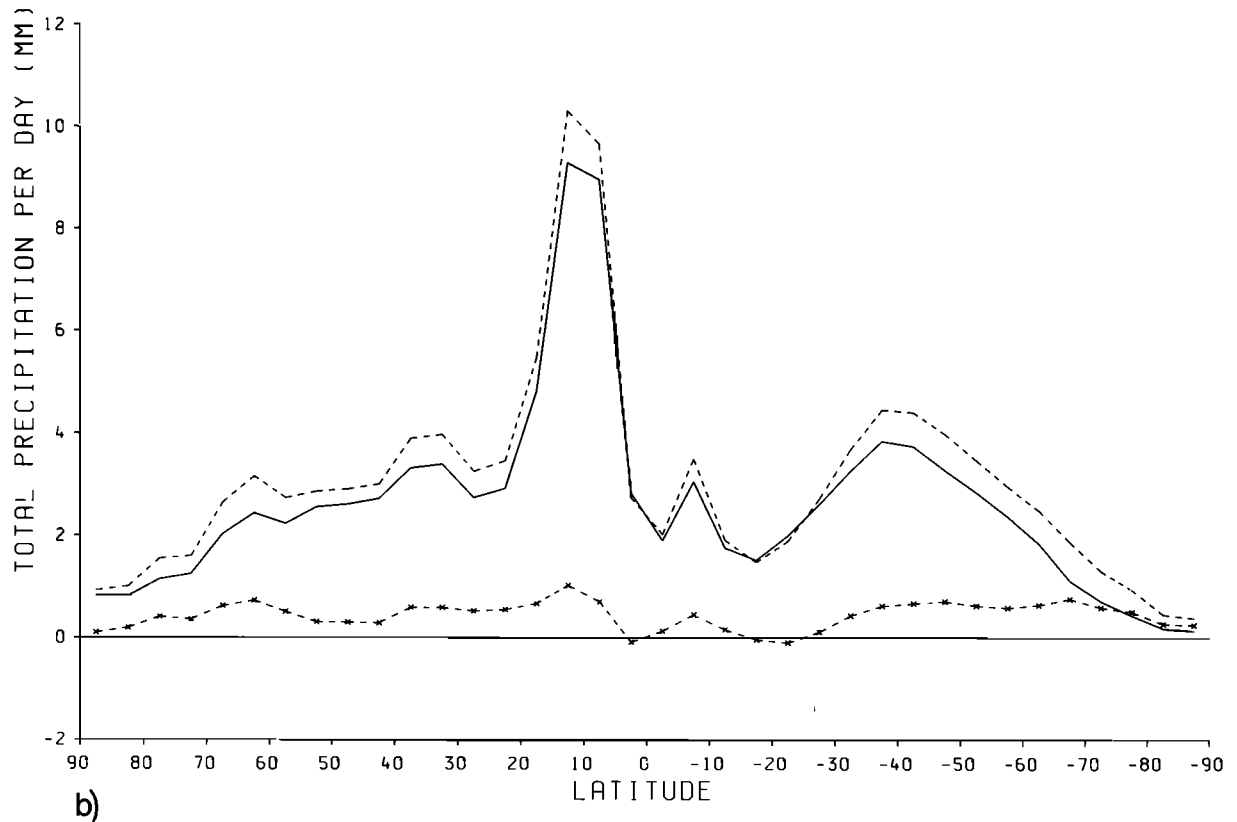


Fig. 15*b*

Fig. 15. Zonal-mean precipitation (in millimeters per day) for control and doubled $CO_2$ experiments meaned over 15 years, and their difference, for (*a*) DJF and (*b*) JJA.

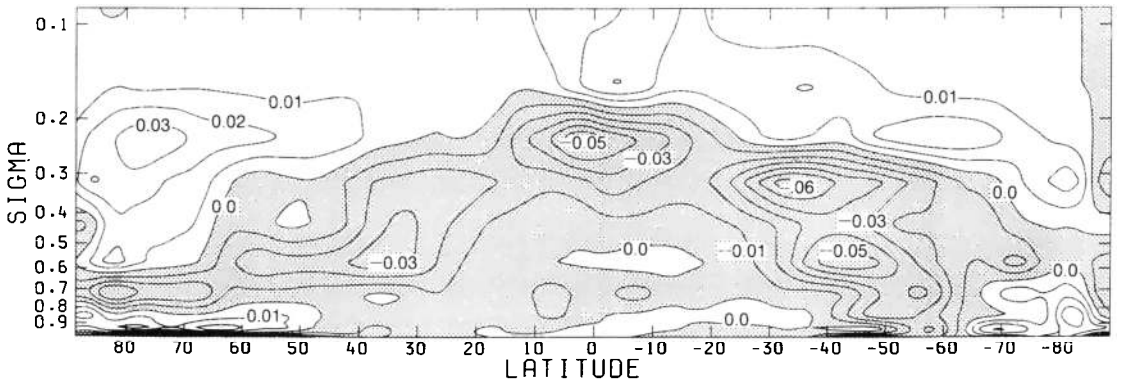


Fig. 16*a*

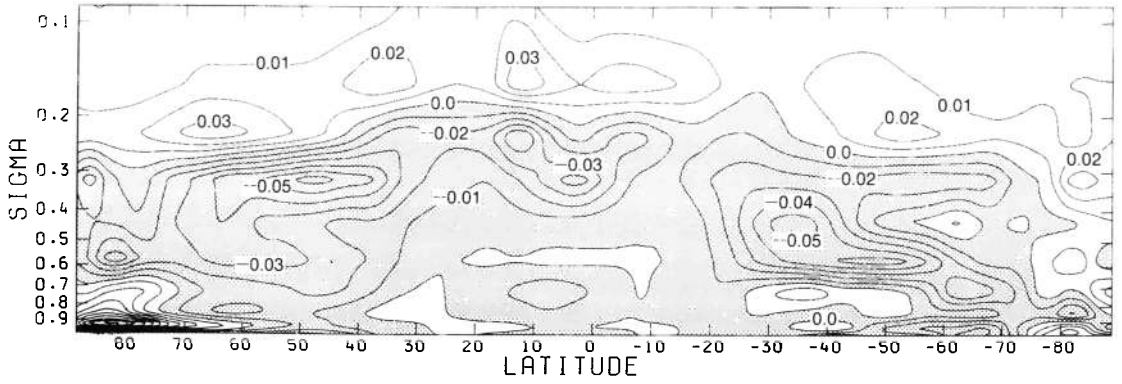


Fig. 16*b*

Fig. 16. Log(sigma)-latitude cross section of difference of zonal-mean layer cloud cover ($2 \times CO_2$ − control, 15-year means, for (*a*) DJF and (*b*) JJA. Contours are at 1% of total cover; decreases are stippled.

*Hansen et al.* [1984]. As with the amplification of temperature increase with height, this is likely to reflect the use of a penetrative convection scheme rather than a moist convective adjustment procedure.

At high latitudes of the northern hemisphere there is increased cloud at lower levels, except in the surface layer. This is to be expected, with increased evaporation from the surface and stable stratification tending to restrict convection to lower levels. The largest temperature increases in the layer next to the surface will tend to reduce the strength of the inversion over land and sea ice in winter and to encourage mixing in the boundary layer to a higher level, and so reduce cloud near the surface. Although this feature is absent from the studies of *Wetherald and Manabe* and *Hansen et al.* (cloud was not allowed to form in the lowest layer of the model used by *Washington and Meehl*, [1984]) and there are quantitative differences in the overall response, the pattern of cloud changes is basically similar to those in the other investigations.

### 5.3 *Geographical Response*

5.3.1 *Temperature.* The largest increases in surface temperature (Figure 17), up to 15°–20°C, are near the sea-ice edge in winter, as was noted in section 5.2. The increases in the tropics, over sea at least, are greater than 3°C but generally less than 4°C. Increases over land are mostly greater than increases over sea at all latitudes, reflecting several different contributions. In northern winter the stable stratification tends to confine the warming to a shallower layer; the removal of snow (not shown) and increased westerly flow into western Eurasia contribute to larger increases; in summer a less cloudy atmosphere allows more solar radiation to heat the surface, whilst the general decrease in soil moisture (discussed later) restricts evaporation so that more of the net radiative heating is balanced by increased sensible heat flux and surface temperatures are higher.

The large increases in temperature over sea ice in winter result from a number of factors which contribute to the sea-ice/temperature feedback. First, melting of sea ice and snow during spring allows more heat from the warmer $CO_2$-enriched atmosphere to be absorbed and stored by the ocean in summer. This leads to a poleward contraction of the ice edge throughout the year and, in these experiments (Table 1), to the almost complete removal of ice during late summer (Figure 18) and autumn. In winter the larger summer heat storage is released and allows greater atmospheric advective heat transport into the regions near the poles. Second, the reduced thickness of ice and lesser depth of snow (a more effective insulator than ice) allows greater heat flux through the ice to maintain a higher surface temperature (although a greater flux will then tend to increase ice thickness). Furthermore, the reduction in the temperature dependent albedo for temperatures above 261.2 K allows more absorption of solar radiation at the surface. Given the weak insolation in winter, the last factor is likely to be least effective. This is clear from the change in surface absorption of solar radiation (Figure 19), which shows large increases in summer where the ice has contracted poleward (see Figure 18) and the

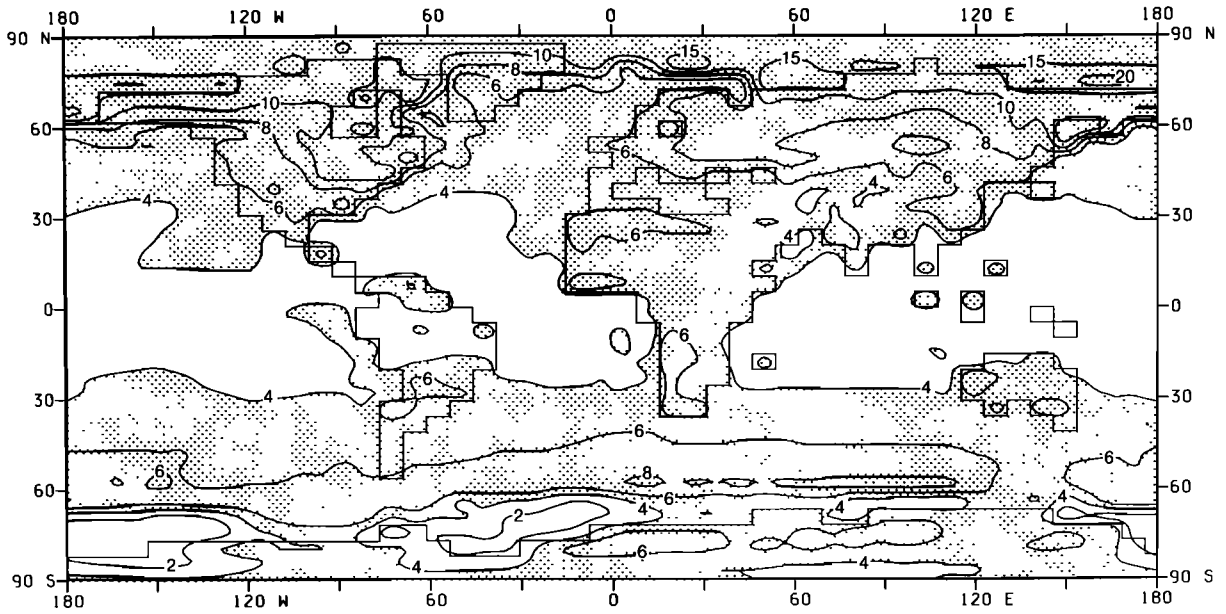


Fig. 17*a*

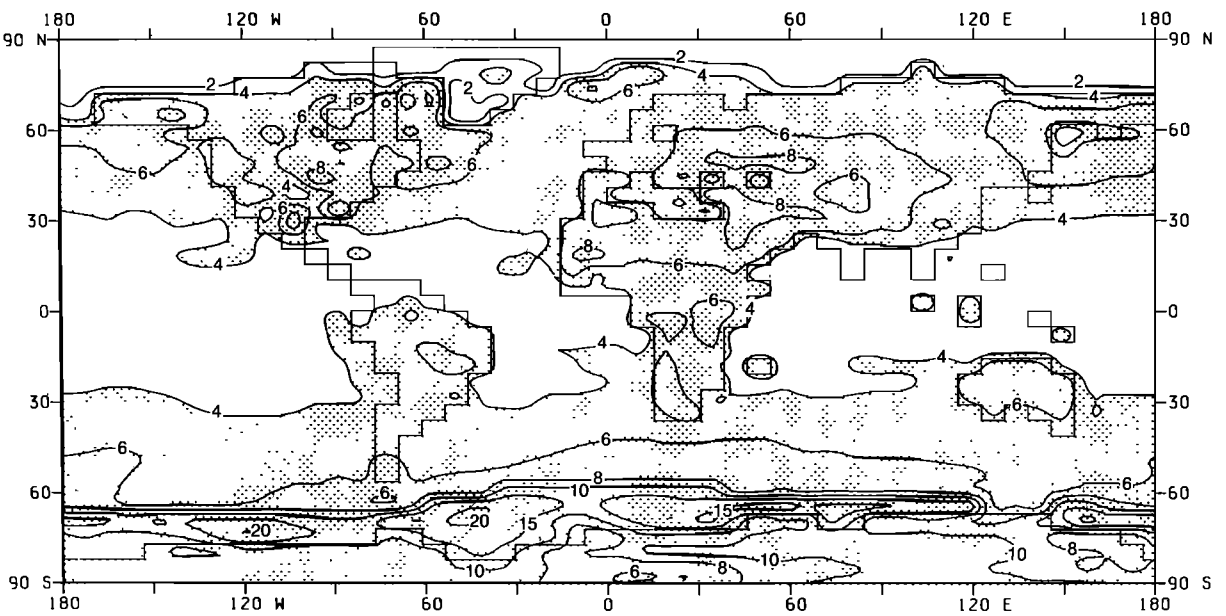


Fig. 17*b*

Fig. 17. Differrences in surface temperature ($2 \times CO_2$ − control, 15-year means) with contours at multiples of 2 K up to 10 K, and then at multiples of 5 K. Increases over 4 K are stippled.

effect of decreased snow cover in northern winter but little change over the poles. In the Arctic in summer, where all the sea ice is removed in the $2 \times CO_2$ experiment, the temperature change is only 2°C because of the large heat capacity of 50 m of water and because in the control the ice is at or close to melting point. The same applies to the Ross and Weddell Seas in summer, where most of the sea ice is removed.

Comparing the changes with results obtained elsewhere with similar models, the tropical temperature increases are larger than those found by *Wetherald and Manabe* [1986] and by *Washington and Meehl* [1984] and similar to those in the study by *Hansen et al.* [1984] (see also *Schlesinger and Mitchell* [1985]); outside the tropics the response is most similar to that obtained by Wetherald and Manabe in both seasons. Although *Hansen et al.* found changes in the northern hemisphere in winter which are qualitatively quite similar, during summer they found land temperature increases only of about 2°–4°C, much less than in this experiment and in the study by Wetherald and Manabe. This is related to the reduction in soil moisture content (see section 5.3.3) found in both the latter investigations but less evident in the former.

In summary, temperature increases range from 2°C over the

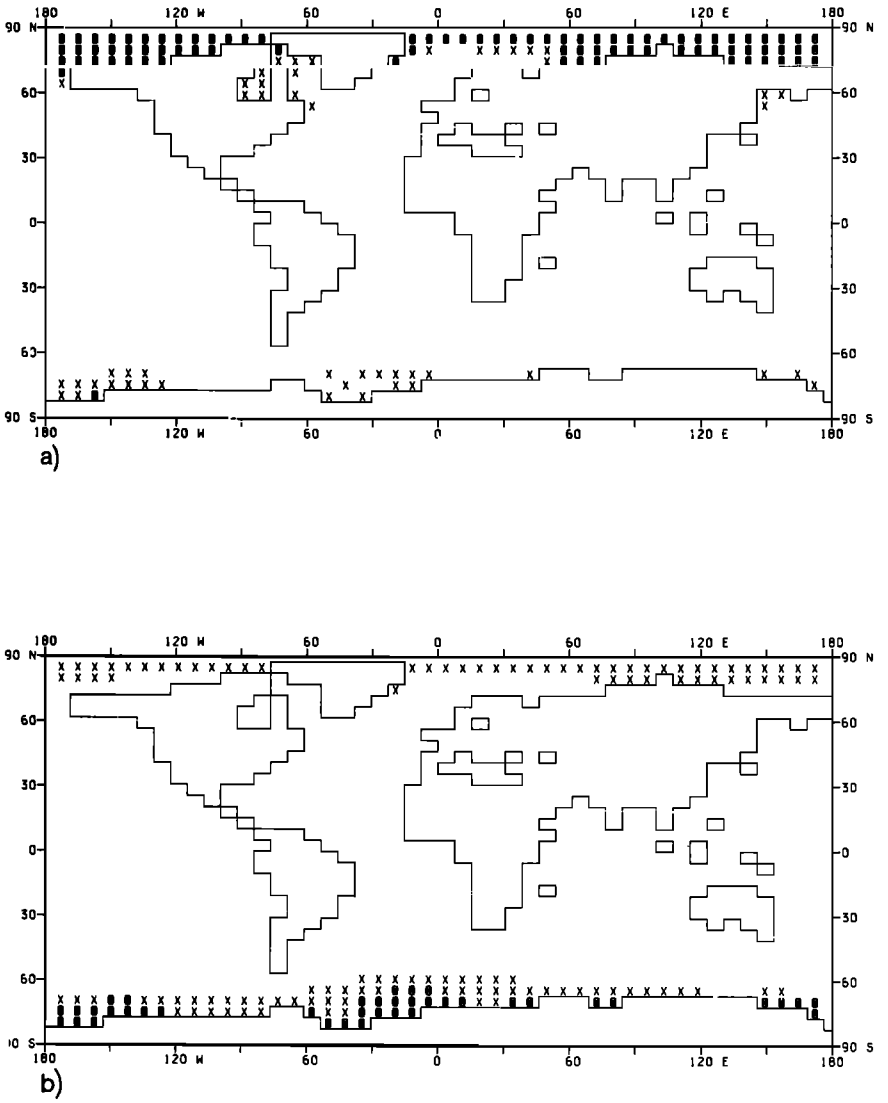


Fig. 18. Sea ice extents (*a*) in February and (*b*) in August for 15-year means of the control experiment (crosses) and the doubled $CO_2$ experiment (open circles). Means are defined as for Figure 11.

summer pole to 20°C over the sea ice of the winter pole; temperatures increase by less than 4°C in the tropics but are 8°–10°C higher over much of the land in the northern hemisphere in winter and 6°–8°C in summer. In the appendix the statistical significance of the changes is assessed against the interannual variability of the model; over most of the globe the changes are significant, at least at the 5% level, and over a very large region at the 1% level.

5.3.2 *Mean sea level pressure.* During December–February there is a reduction in sea level pressure (Figure 20*a*) over the Arctic, especially over Baffin Bay, the Norwegian Sea, and off Kamchatka, where there is substantially less sea ice than in the control simulation (Figure 18*a*). *Mitchell and Hills* [1986] also found significant reductions in pressure where sea ice was removed in a prescribed anomaly experiment. To the south there are increases over much of the North Atlantic and southern Europe, giving enhanced westerly flow into northern Europe and Asia. Increased westerly flow over Europe (and also northern Canada) in winter and spring was also evident in previous $CO_2$ studies with prescribed sea surface temperature increases using a different model [*Mitchell*, 1983; *Mitchell and Lupton*, 1984].

There are substantial reductions in the subtropics in southern hemisphere summer and a similar but more pronounced response in the northern hemisphere during June–August (Figure 20*b*). These changes may be larger in northern hemisphere because of the greater atmospheric warming (compare Figures 13*a* and 13*b*), particularly near 30°–40° of latitude in the summer hemisphere. Note also the increases in sea level pressure over the western tropical Pacific and the extreme southeast of Asia, which are associated with a northward shift of the models' ITCZ, discussed in section 5.3.3.

Pressure increases in southern high latitudes in winter (Figure 20*b*), probably because of mass displaced from the northern hemisphere. Note that the rises are a minimum along the new sea-ice edge (Figure 18*b*), consistent with the findings of *Mitchell and Hills* [1986].

5.3.3. *Precipitation and soil moisture.* Precipitation is

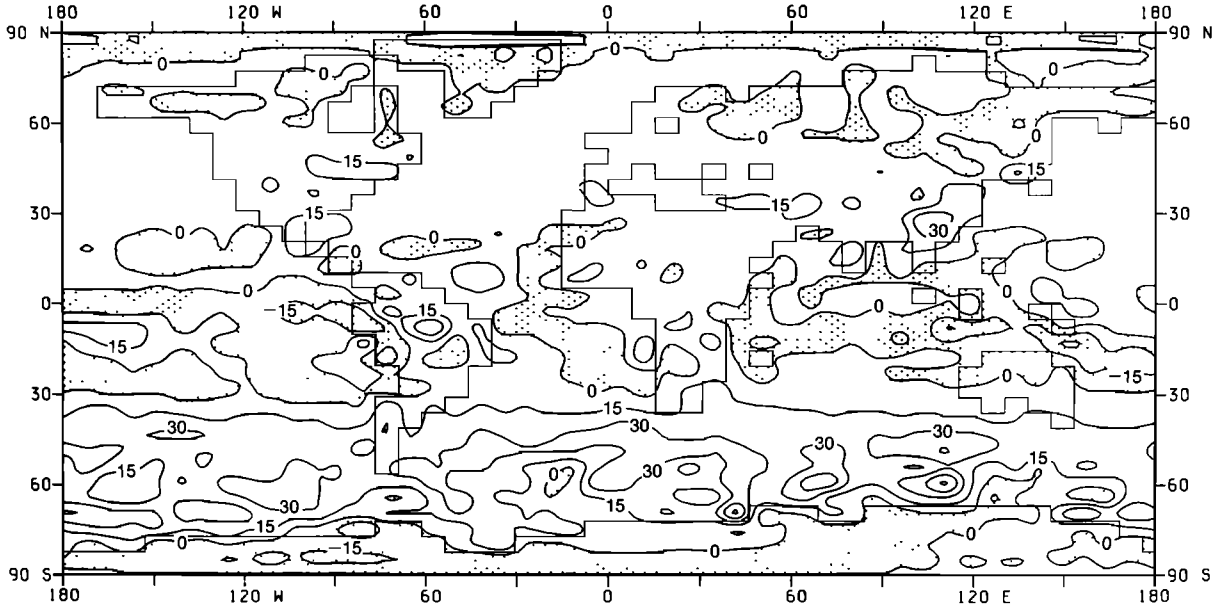


Fig. 19*a*

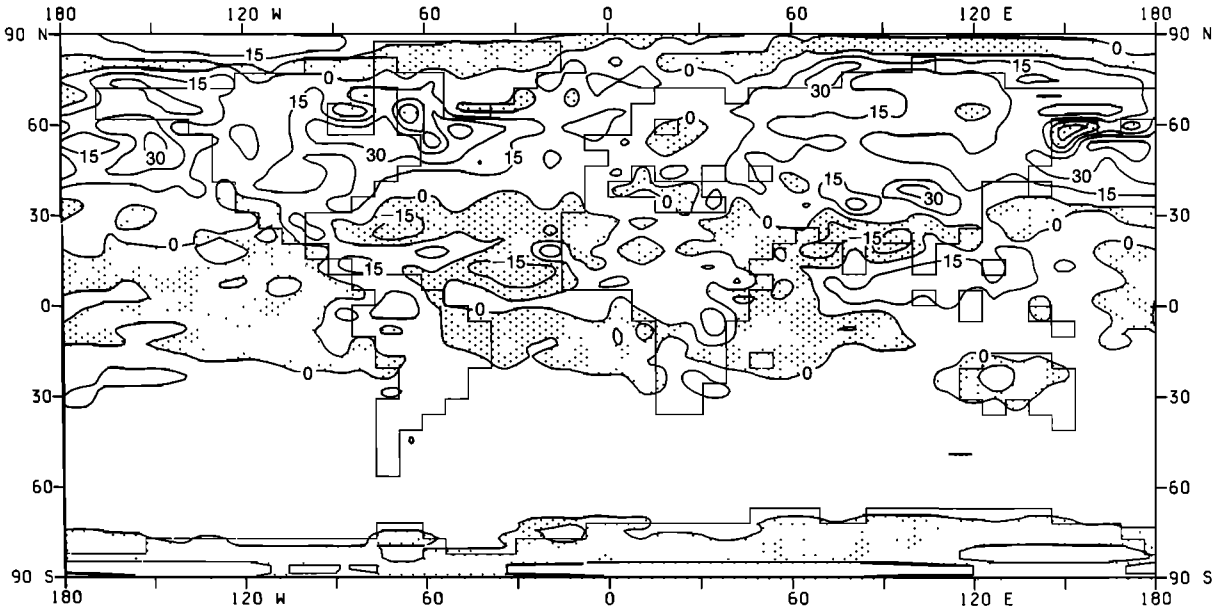


Fig. 19*b*

Fig. 19. Differences in solar radiation absorbed at the surface ($2 \times CO_2$ − control, 15-year means) with contours at 0 and multiples of ±15 W $m^{-2}$ and decreases stippled for (*a*) DJF and (*b*) JJA.

greater at high latitudes in both seasons (Figure 21); the largest increases are along the depression tracks and are consistent with increased moisture convergence due to a higher atmospheric moisture content. In winter at high latitudes, this increased precipitation occurs as snow and increases the snow depth over Asia in particular (not shown). In northern summer (Figure 21*b*) the precipitation is greater along the ITCZ over the central and east Pacific, the Atlantic, and into west Africa. The Asian monsoon is strengthened, and there are decreases over the west Pacific, southeast Asia, and the Indian Ocean, north of the equator. There is decreased rainfall in the already dry north African region and extensive reductions over southern Europe and mid-latitudes of Asia. In DJF (Figure 21*a*) the pattern of changes shows a general shift southward of rainbelts in the tropics and southern hemisphere, with increases over central South America, central southern Africa, the Indian Ocean, northern Australia, and the southwest and central southern Pacific, with decreased precipitation generally to the north of the rainbelt. Elsewhere in the tropics the pattern is less clear; e.g., there are increases in the east Pacific north of the equator in the main precipitation band (cf. Figure 5*a*) but decreases over Mexico and nearby and over the east Atlantic north of the equator. Along the equator in the eastern Pacific, which was a rainfall minimum in the control (Figure 5*a*) there is increased

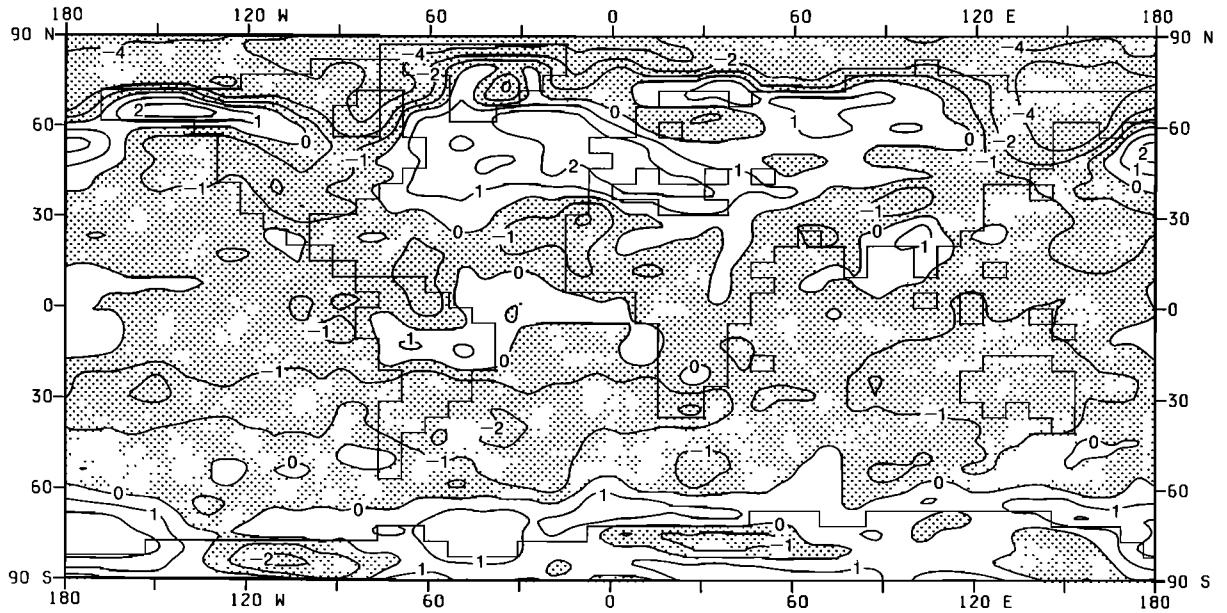


Fig. 20*a*

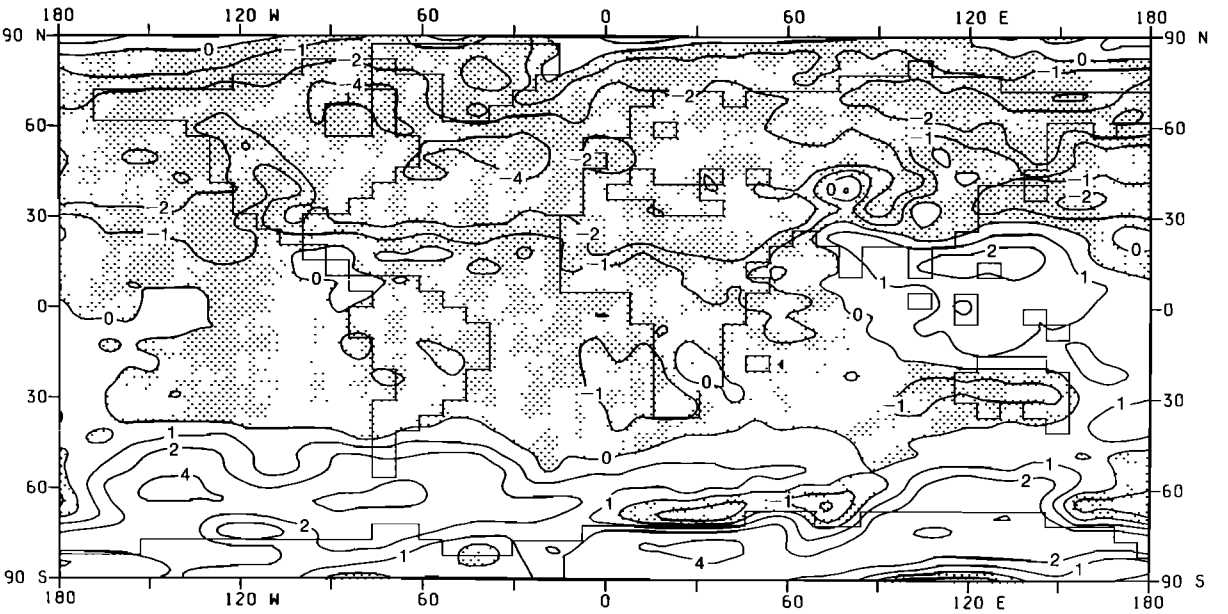


Fig. 20*b*

Fig. 20. Differences of pressure reduced to mean sea level ($2 \times CO_2$ − control, 15-year means) for (*a*) DJF and (*b*) JJA. Contours at ±1 mbar, ±2 mbar, and multiples of 4 mbar, decreases are stippled.

precipitation. In JJA the pattern of changes shows some shifts northward of the main rainbelts, with the strengthening of the Asian monsoon the most noticeable, but the pattern is generally less consistent than the southward shift in DJF. Such a northward movement could be due to increased heating over land in summer (see Figures 19*b* and 23*c*) because of reduced cloud.

Although the other studies with similar models were all in agreement with the increases at high latitudes, there were considerable discrepancies in the tropics and over land in mid-latitudes in JJA. In this respect our results, with the decreases over Europe and much of Asia and the increased monsoon circulation, are most like those obtained by Wetherald and Manabe [see *Schlesinger and Mitchell*, 1985]. They are also similar to our results with higher-resolution models with prescribed cloud [*Mitchell and Lupton*, 1984; *Mitchell et al.*, 1987] and model-generated cloud [*Mitchell et al.*, 1986], although there are differences, for example, over the tropical oceans during DJF.

Soil moisture increases over much of northern Europe, northwest and central Asia, and the western United States and Canada in DJF (Figure 22*a*, cf control simulation Figure 22*c*). In the southern hemisphere there are increases near 15°S. In JJA (Figure 22*b*; cf. control Figure 22*d*), soil moisture decreases

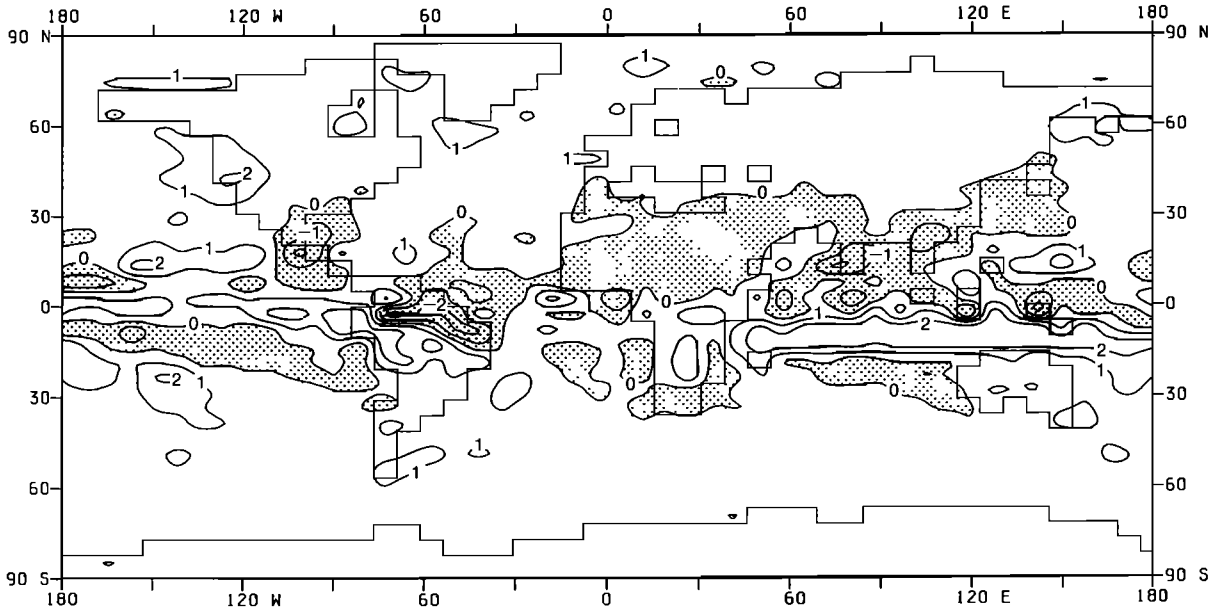


Fig. 21*a*

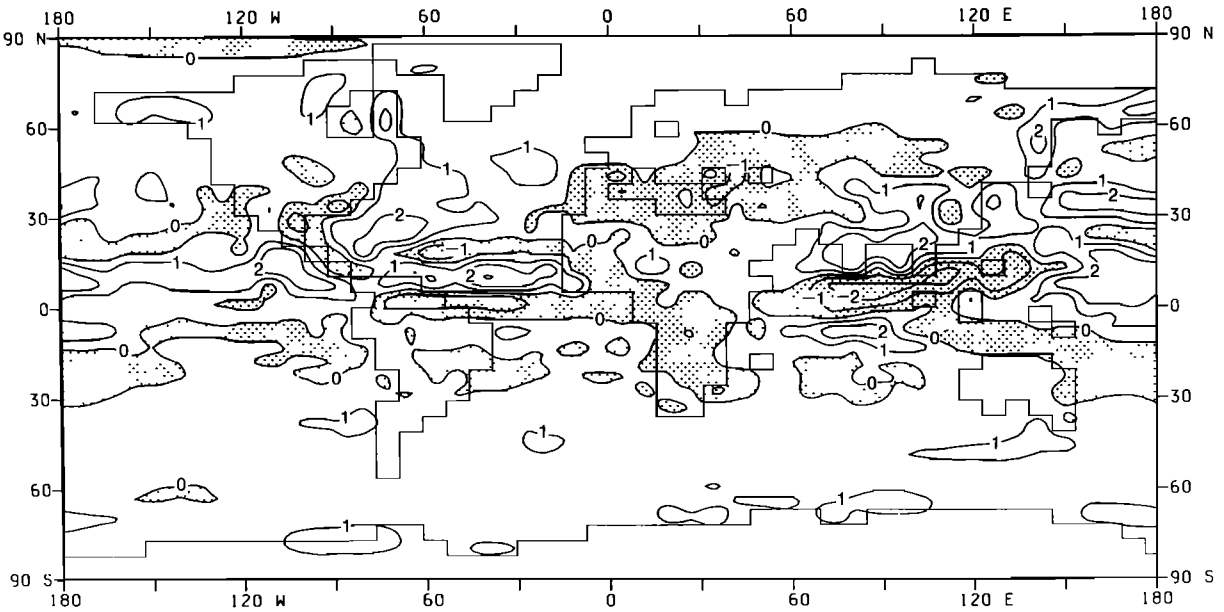


Fig. 21*b*

Fig. 21. Precipitation changes ($2 \times CO_2$ − control, 15-year means), with contours at 0, ±1 and ±2 mm $day^{-1}$, and decreases stippled for (*a*) DJF and (*b*) JJA.

over most areas except India and southern Asia, west Africa, and northern Mexico, where there is increased precipitation from monsoon circulations. The drying of the land in the northern hemisphere is similar to the results of the Meteorological Office experiments with higher resolution [for example, *Mitchell, 1983, 1986*] and those with Geophysical Fluid Dynamics Laboratory (GFDL) models [see *Manabe and Wetherald*, 1986; *Schlesinger and Mitchell*, 1985]. The mechanism for the drying in this experiment is similar to that found by *Manabe et al.* [1981]. At latitudes north of 45°N the spring snowmelt and runoff start and end earlier in the warmer climate (Figures 23*a* and 23*b*), so the summer drying season is longer and more solar radiation is absorbed and is available to increase evaporation because of the earlier removal of highly reflective snowcover (Figure 23*c*). To the south of this region the reductions in precipitation and cloud enhance the winter to summer seasonal drying. There is a corresponding increase in absorption of solar radiation between 30° and 55°S from November to March (Figure 23*c*) because of the large reductions in cloud (see Figure 16*a*). The zonal mean changes of soil moisture through the year (Figure 24) show a pronounced drying in summer centered near 50°N. The pattern of changes is very much like that obtained by *Manabe and Wetherald* [1986], although there is a pronounced drying along the equator in our

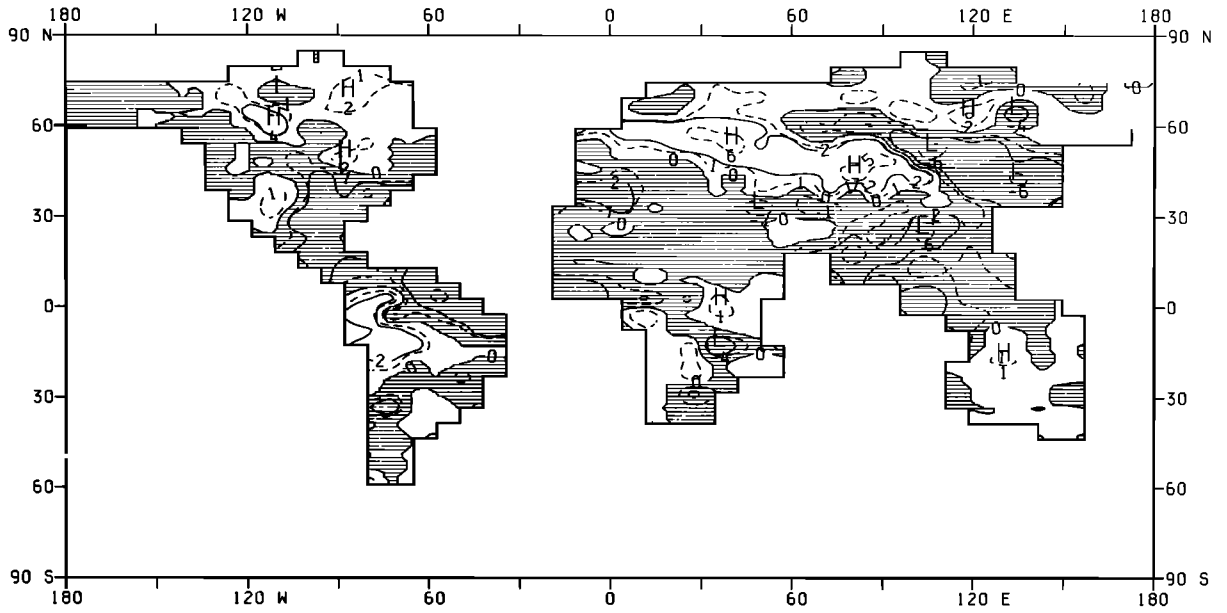


Fig. 22*a*

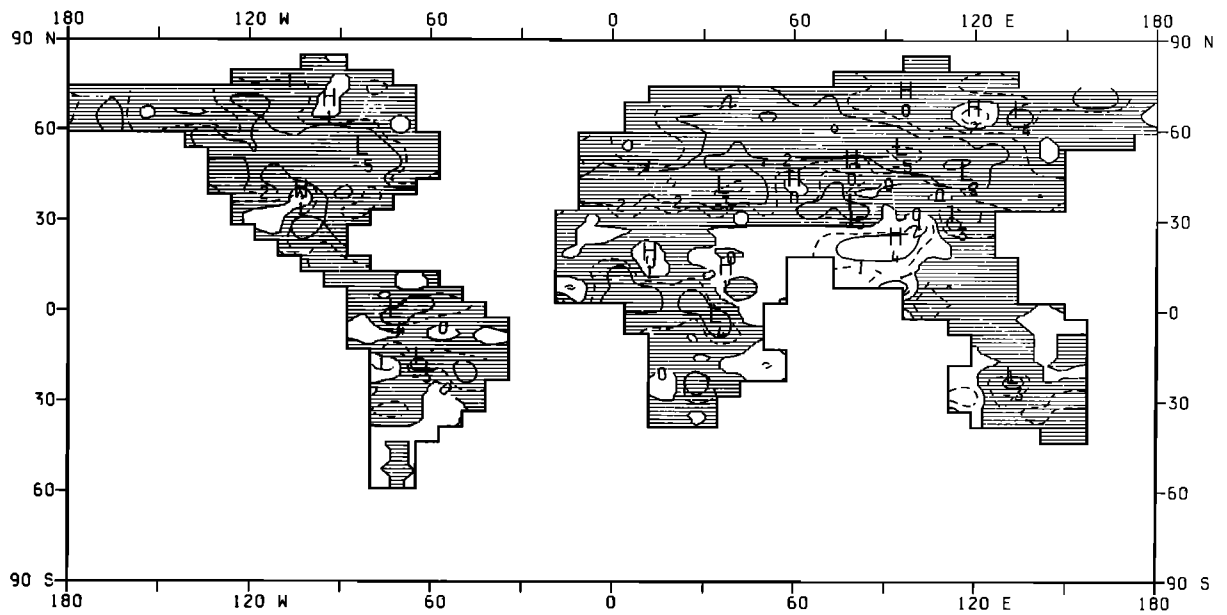


Fig. 22*b*

Fig. 22. As in Figure 20, but for soil moisture content, with contours at 0, ±1, ±2, ±5 and ±10 cm, and decreases shaded. (*a*) DJF. (*b*) JJA. Soil moisture for control for (*c*) DJF and (*d*) JJA, with contours at 0.3, 1.25, 2.5, 5, 10, and 14.5 cm, and shaded below 5 cm.

experiment, whereas there is little change in soil moisture here in their model; the model used by *Hansen et al.* [1984] produced increases both near 60° N and the equator [see *Schlesinger and Mitchell*, 1985]. Another difference from these two studies is the band of inerease in summer and autumn near 20° N (see Figure 24); this reflects the increases in monsoon areas, which, despite generally larger changes in precipitation in the *Wetherald and Manabe* [1986] study [see *Schlesinger and Mitchell*, 1985], are not in general accompanied by increased soil moisture.

## 6. SUMMARY AND CONCLUSIONS

The sensitivity of global climate to doubled atmospheric $CO_2$ has been investigated using a global general circulation model coupled to a simple mixed layer ocean model and a thermodynamic sea-ice model. The depth of the ocean was sufficient to model the seasonal storage and release of heat. Transport of heat by the oceans was allowed for by specifying a seasonally varying heat convergence.

A control integration of 20 years with the present level of $CO_2$ reached a state reasonably close to equilibrium after 7 years and

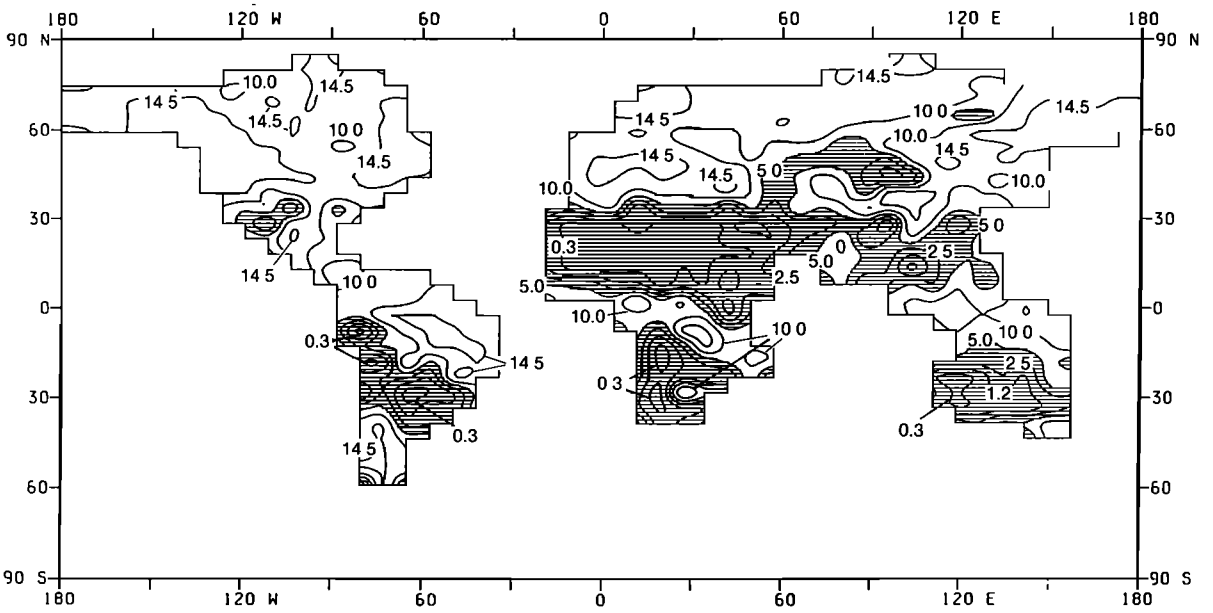


Fig. 22*c*

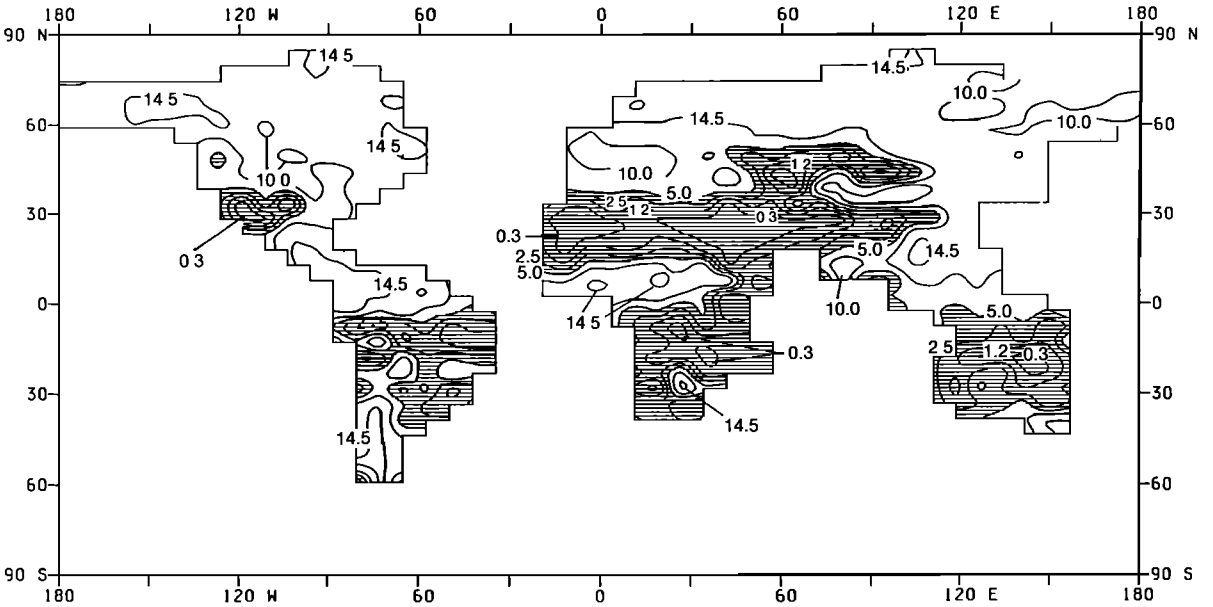


Fig. 22*d*

simulated well many features of the observed climate. The prescribed heat convergence in the ocean ensured that both sea surface temperatures and the seasonal variation of ice were in close agreement with observations. The zonally meaned distribution of clouds generated by the model is qualitatively similar to observed estimates. Overall, the simulation of present climate is at least as good as in the published results from other models used to study the sensitivity to enhanced $CO_2$.

The anomaly integration, with $2 \times CO_2$, attained a state in reasonable equilibrium by year 38. No attempt was made to accelerate the approach to equilibrium. The global mean surface temperature increased by 5.2°C, slightly larger than in recent similar studies elsewhere. As discussed earlier the main reasons for a larger warming are probably the use of a penetrative convection scheme rather than a moist convective adjustment procedure and the larger cloud temperature feedback due to not restricting the formation of cloud at high levels. Zonal mean tropospheric temperatures are warmer by 4°C or more nearly everywhere, with increases of up to 8°C in the upper tropical troposphere. The tendency of the model to adjust the vertical profile toward the moist adiabatic lapse rate leads to the vertical amplification of the warming, which is probably larger owing to the use of the penetrative convection scheme rather than a moist convective adjustment procedure used in some other models. At higher latitudes in winter the stable profile mainly confines the largest warming to the surface and lower troposphere. Zonal mean westerly wind is stronger at upper levels in the tropics and generally decreased outside low latitudes, which is consistent

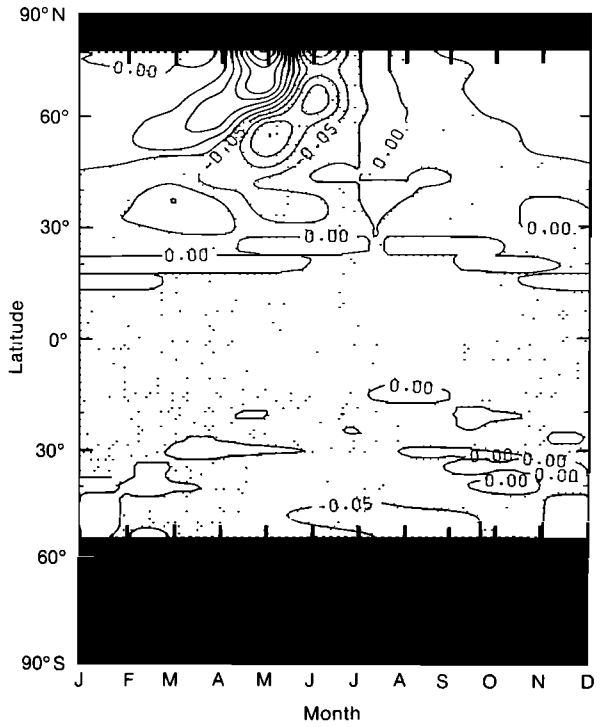


Fig. 23a

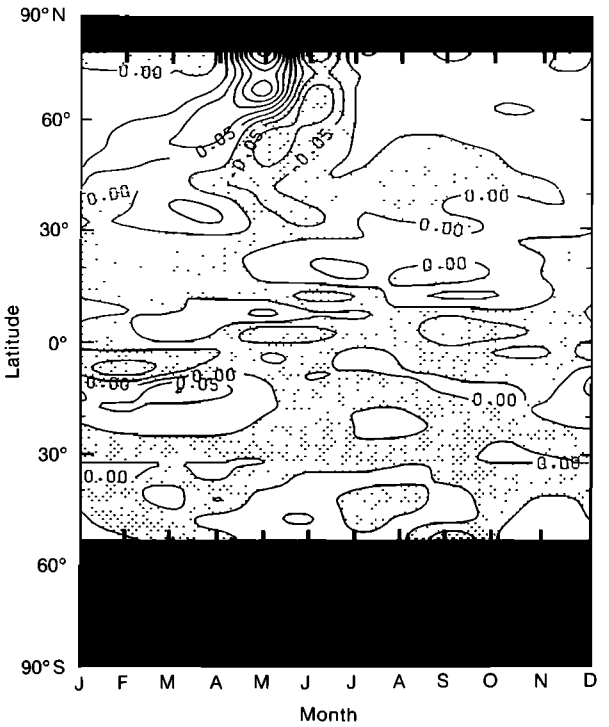


Fig. 23b

Fig. 23. Time-latitude diagrams of difference of zonal mean over land of (*a*) snowmelt, (*b*) runoff (both with contour interval 0.05 cm day$^{-1}$, and decreases stippled), and (*c*) surface absorption of solar radiation (contour interval, 10 W m$^{-2}$, decreases stippled) in the doubled $CO_2$ experiment from the control experiment.

with the respectively increased and decreased meridional temperature gradients.

The global mean moisture content of the atmosphere increases by 41% and precipitation increases by 15%. Zonally averaged precipitation increases almost everywhere except in the subtropics during winter, with largest increases in the main convergence zones of the equatorial trough and middle and high latitudes. The broad pattern of zonal mean cloud changes is similar to that found in the Meteorological Office model at higher resolution with prescribed sea surface temperatures [*Mitchell et al.*, 1986] and to that found elsewhere [see *Wetherald and Manabe*, 1986]; there is a general decrease in middle-level clouds, increased high cloud at all latitudes, and some increases in low cloud at high latitudes. The decrease in relative humidity in the midtroposphere and increase above is consistent with a raised tropopause and deeper convection.

The surface temperature increase varies geographically from less than 2°C where sea ice has melted in the Arctic in summer, and from 3° to 4°C over tropical oceans to 15° to 20°C over winter sea ice. Over land in the northern hemisphere, increases are mostly 6°–8°C in summer and 8°–10°C in winter. At high latitudes the thinner ice and reduction in snow contribute to the warming, as does the release of greater heat stored in the ice-free ocean during the previous summer. The reduction in snow and increased westerly flow into Europe contribute to the winter warming, whilst the reduction in soil moisture and cloud give the large warming over much of northern hemisphere land in summer. Here spring snowmelt and runoff start and end earlier, so that the drying season is longer and, with reductions in cloud and precipitation in some areas, more pronounced, so drying out much of the land. Similar reductions in soil moisture have been found in previous Meteorological Office experiments and are broadly in agreement with the results of *Manabe and Wetherald* [1986].

In broad terms there is a fair amount of agreement between

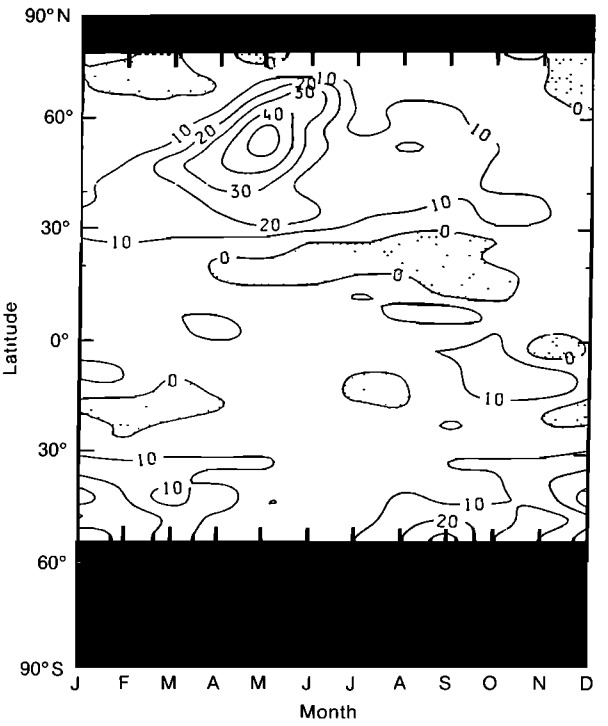


Fig. 23c

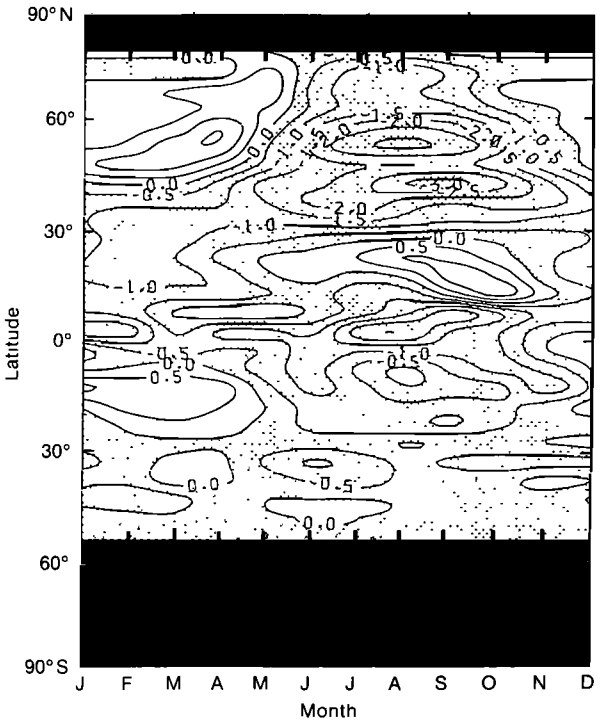


Fig. 24. As in Figure 23, but for soil moisture content, with contour interval of 0.5 cm and decreases stippled.

our results and the similar studies of *Hansen et al.* [1984], *Washington and Meehl* [1984], and *Wetherald and Manabe* [1986], especially with respect to zonal mean changes. However, there are some important differences, some of which may be due to the different treatments of convection and the land surface or to differences in the control climate simulations [*Mitchell et al.*, 1987]. All of the studies obtain warmings of 4° or 5°C, with reduction in cloud probably being the major reason for enhanced warming compared to earlier studies with fixed clouds.

We have described the time-averaged response of a three-dimensional climate model to a doubling of atmospheric $CO_2$ concentrations. Detailed analyses of both the changes in cloud cover and in temporal variability will form the subject of future papers. An additional experiment in which $CO_2$ was doubled and sea ice extents were prescribed, as in the control simulation, will be reported later.

Finally, in order to identify topics which are a priority for future work, it is instructive to consider the limitations of the present work and other similar studies.

1. The representation of cloud is extremely crude, and studies to date take no account of possible changes in cloud optical properties. *Somerville and Remer* [1984] have revived speculation that cloud water and hence cloud reflectivities would increase in warmer, moister atmosphere, providing a significant negative feedback which would reduce the sensitivity of climate to increased atmospheric $CO_2$. A parameterization of cloud water has been developed [*Smith*, 1985] and will be used in future studies of enhanced $CO_2$.

2. The dynamics of sea ice and changes in ocean dynamics are not taken into account. Numerical simulations indicate that the inclusion of ice dynamics would enhance the seasonal variation in sea-ice cover [*Hibler*, 1984]. Nevertheless, the present model produces an accurate simulation of the seasonal amplitude of ice extent variations, although this was found to be sensitive to the specification of the surface albedo. It is possible that temperature albedo feedback over sea ice is excessive, compensating for the lack of sea-ice dynamics to give a realistic annual variation but producing an unrealistically large response in the enhanced $CO_2$ integration. The neglect of changes in ocean circulation may not lead to serious errors, as experiments with an idealized coupled ocean atmosphere [*Manabe and Bryan*, 1985] suggest that the strength of the oceanic meridional circulation changes little on increasing atmospheric $CO_2$. However, a more detailed model of the ocean than that used here will be needed to estimate the time dependent response of climate to the observed gradual increase in $CO_2$ and other trace gases. A version of the Meteorological Office 11-layer atmospheric model has been coupled to a dynamical model of the ocean for use in further studies of the equilibrium and transient response to enhanced $CO_2$ concentrations.

3. The horizontal resolution used in this study and elsewhere does not represent adequately the weak baroclinic disturbances characteristic of northern mid-latitudes in summer. The present work needs to be repeated at higher resolution to ensure that features such as the drying of the northern mid-latitude continents in summer are not artifacts of the low resolution used.

4. Although the parameterization of some physical processes (for example, radiation) can be validated against detailed theoretical models, others (including convection and the representation of cloud and land surface) contain arbitrary assumptions and constants which cannot be verified directly against theory or measurement. We have seen that models using a penetrative convection scheme produce a much larger warming in the upper tropical troposphere with increased atmospheric $CO_2$ than do models using moist convective adjustment. An investigation of the effect of changes in the Earth's orbital parameters, currently in progress in the Meteorological Office, indicates that the simulated changes in precipitation over the subtropical continents are sensitive to the prescription of evaporation. We plan to repeat the present study using a revised parameterization of the land surface to determine if the response of the present model is sensitive to such model changes in formulation.

It is clear that we are still some way from predicting the magnitude and distribution of climate change due to increased atmospheric $CO_2$ with the accuracy required for climatic impact studies. Experiments such as that reported here should be regarded as sensitivity studies and not as forecasts. These sensitivity studies indicate the mechanisms which are likely to be important as climate changes and identify those processes which must be modeled accurately. There is still much work to do in this direction.

## APPENDIX: STATISTICAL SIGNIFICANCE OF CHANGES IN SURFACE PRESSURE, SURFACE TEMPERATURE, PRECIPITATION AND SOIL MOISTURE

Climate simulations made with three-dimensional models exhibit random fluctuations from year to year in a similar way to the observed climate. Some of the differences between the anomaly and control integrations described earlier may therefore have arisen by chance. A simple significance test has been used to determine those changes unlikely to occur by chance and which are probably due to increased $CO_2$.

A two-tailed Student's t-test was carried out on the DJF and

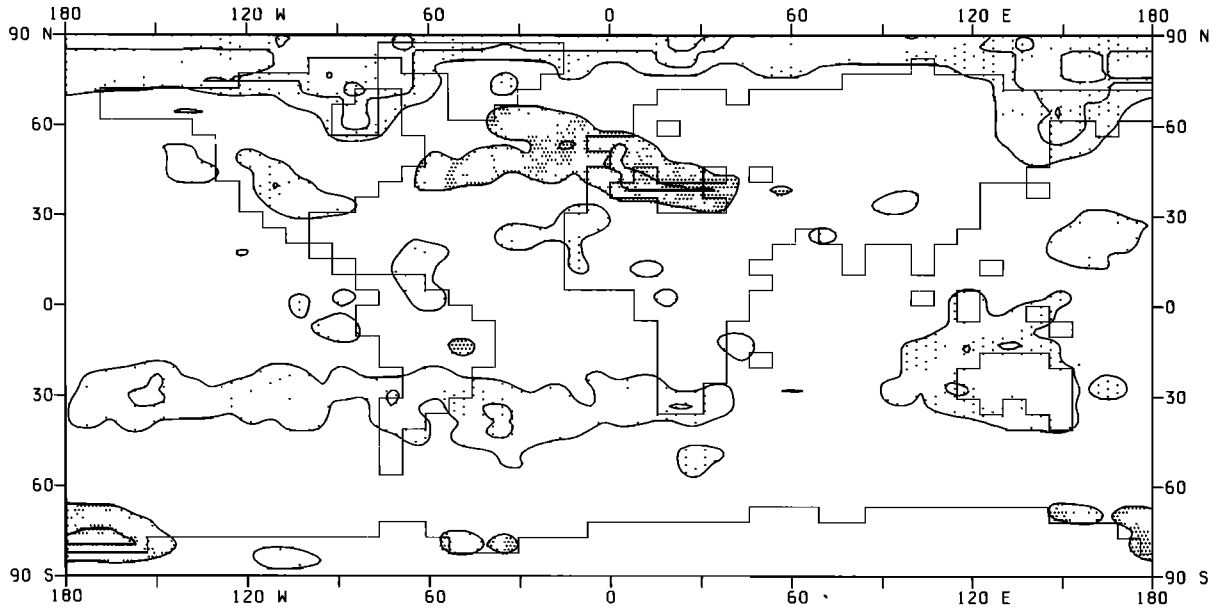


Fig. 25*a*

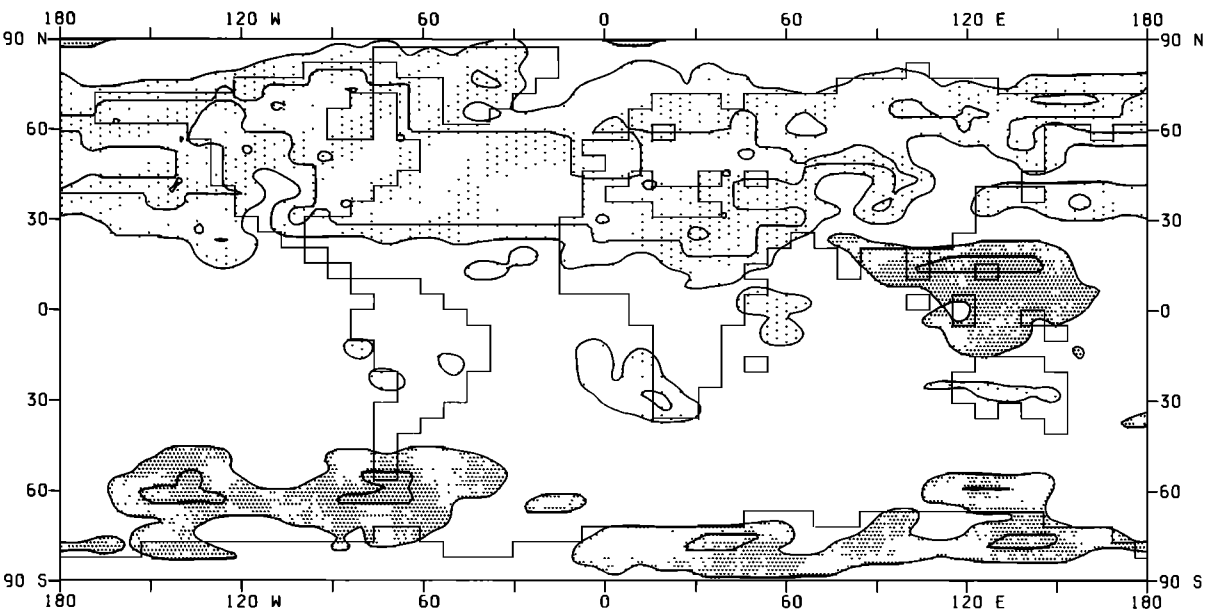


Fig. 25*b*

Fig. 25. Student's t-statistic for changes in pressure reduced to mean sea level between doubled $CO_2$ and control experiments in (*a*) DJF and (*b*) JJA, contoured at 10%, and 1% significance levels for two-tailed tests, with changes significant at the 10% level stippled, light for decreases and dark for increases.

JJA seasonal means from the last 15 years of control and anomaly for each of the changes in surface pressure, surface temperature, precipitation, and soil moisture. The limitations of such a test applied to meteorological variables which are correlated in space and which may not be sampled from a normal population (especially true of precipitation [*Reed*, 1986]) have been noted by *Mitchell et al.* [1987]. The tests should be viewed as confirming those aspects of the model response for which a physical explanation can be given.

Charts of the t-statistic show that the increase in pressure over the north Atlantic and Europe in DJF (Figure 25*a*) and the decreases over the north pole and in the subtropics in the southern hemisphere are significant, at least at the 90% level of confidence. In JJA (Figure 25*b*) the general fall in pressure over the northern hemisphere is mostly significant at the 95% level and in much of the region at the 99% level, as is the increase in pressure over southeast Asia and the west tropical Pacific.

The surface temperature increase is significant at the 99% level of confidence almost everywhere in both DJF and JJA (not shown), as might be expected from the large warming compared

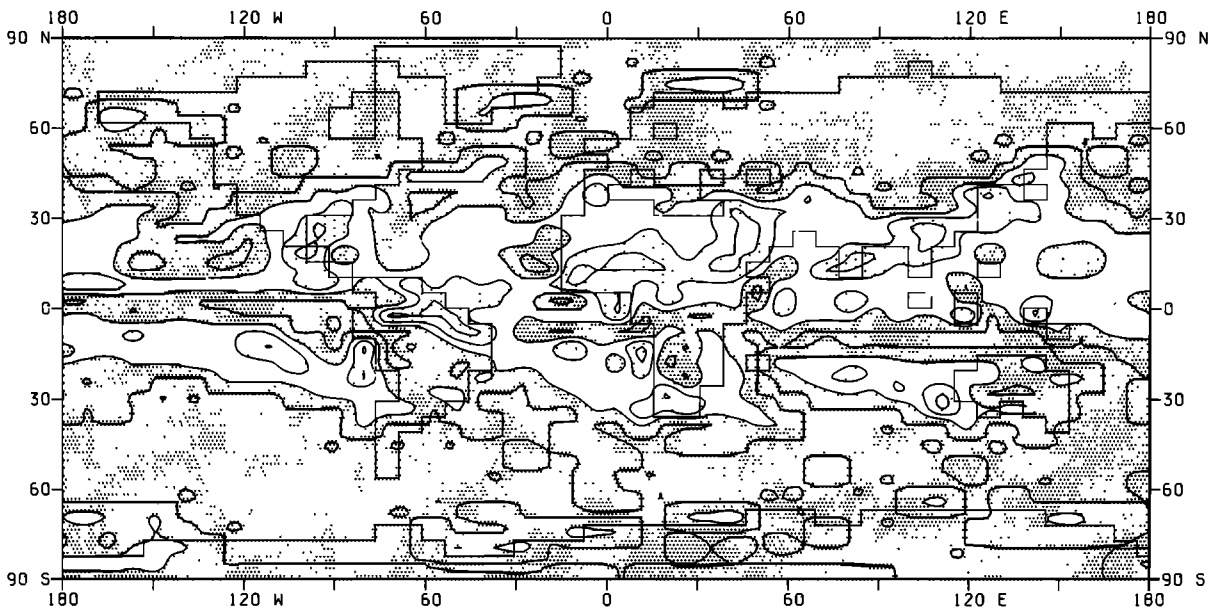


Fig. 26*a*

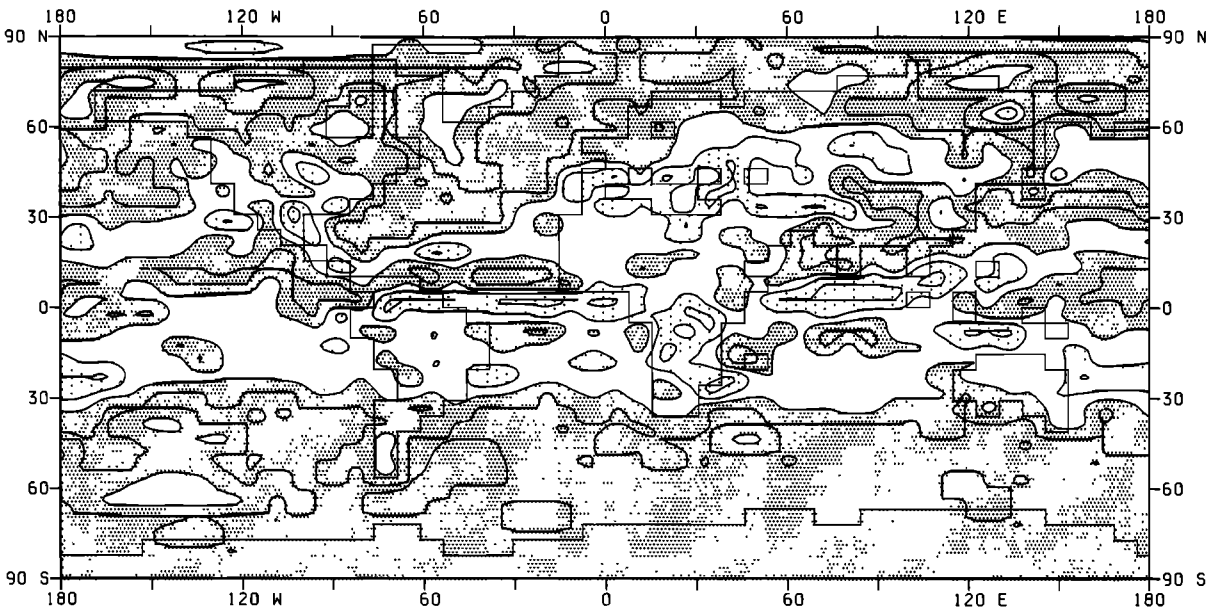


Fig. 26*b*

Fig. 26. As in Figure 25, but for precipitation.

to interannual seasonal variability. Precipitation is inherently more variable spatially, and so one might expect a smaller total area of significant changes and a less coherent pattern. However, the increases at high latitudes in both seasons (Figure 26) are mostly significant at the 95% level or higher, as is the southward shift of the main precipitation bands in DJF and also the northward shift and strengthening of the monsoon rainfall in JJA. The decreases in the winter subtropics and over southern Europe and Asia in JJA are also significant in many areas.

The t-statistic for changes in soil moisture, which tends to have a large interannual variability, even so shows that the major changes such as a wetter surface over parts of Canada, and northern Europe and Asia in DJF and the drying of northern hemisphere land in summer are mostly significant at the 90% level of confidence or higher (Figure 27).

The greater length of the integrations compared to previous studies with prescribed sea surface temperatures has enabled tests with more degrees of freedom to be performed. The high level of significance of many of the changes here, which are similar to previous results, encourages the belief that the model's true response to enhanced $CO_2$ has been identified.

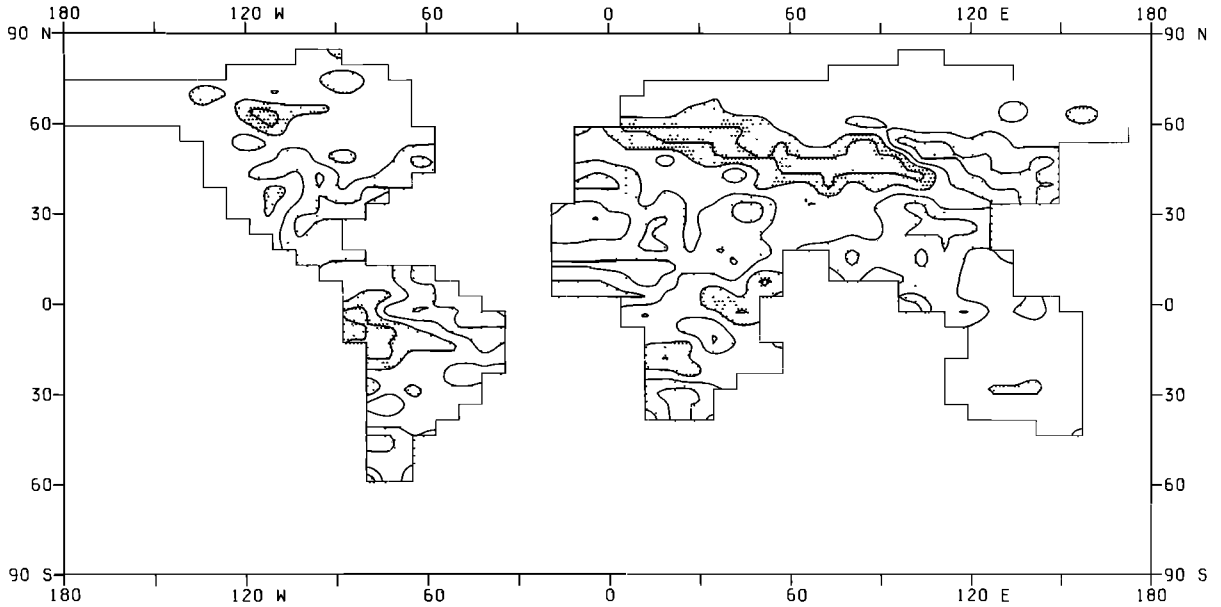


Fig. 27*a*

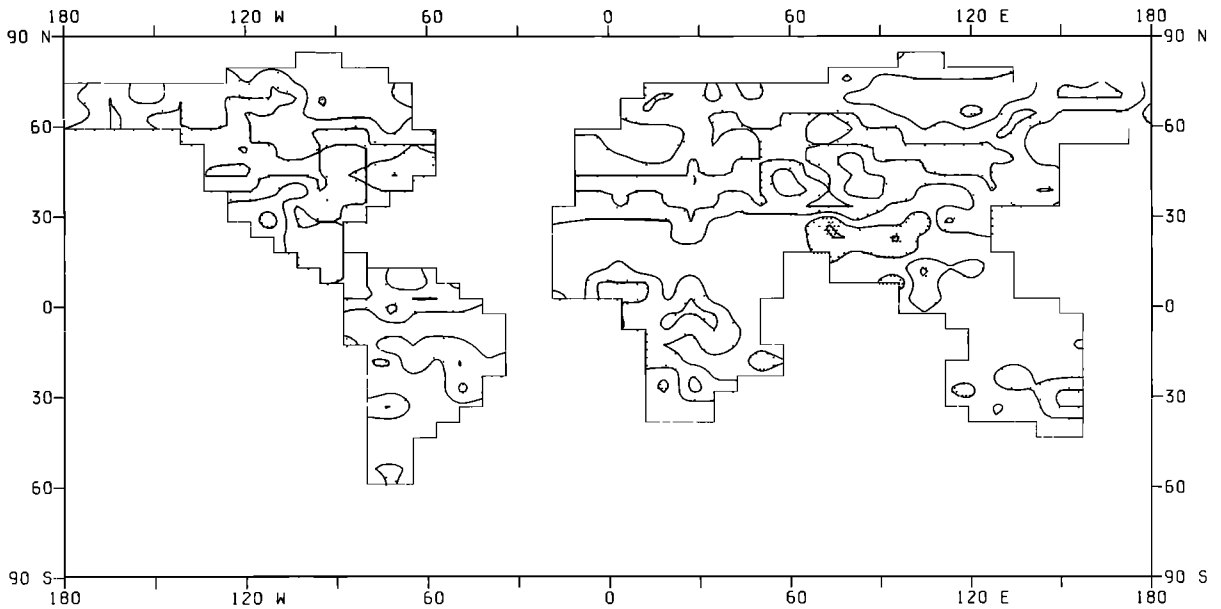


Fig. 27*b*

Fig. 27. As in Figure 25, but for soil moisture content

*Acknowledgments.* We are indebted to Bob Wilderspin for assistance and advice in adapting the cloud and convective parameterizations for use in the low-resolution climate model. William Ingram helped in the development of the mixed layer model, and Kevin Needham obtained the diagrams. Peter Rowntree reviewed early versions of the manuscript and some minor revisions suggested by two referees have been incorporated. This work was supported in part by the European Economic Commission through contract CL-114-UK(H).

## REFERENCES

Alexander, R. C. and R. L. Mobley, Monthly average sea surface temperatures and ice pack limits on a 1° global grid, *Mon. Weather Rev.*, *104*, 143–148, 1976.

Clarke, R. H., Recommended methods for the treatment of the boundary layer in numerical models, *Aust. Meteorol. Mag.*, *18*, 51–73, 1970.

Crane, R. G. and R. G. Barry, The influence of clouds on climate with a focus on high latitude interactions, *J. Climatol.*, *4*, 71–93, 1984.

Cunnington, W. M. and P. R. Rowntree, Simulations of the Saharan atmosphere-dependence on moisture and albedo, *Q. J. R. Meteorol. Soc.*, *112*, 971–999, 1986.

Gordon, C. and M. Bottomley, A scheme for incorporating the thermodynamic sea-ice model into a coupled ocean-atmosphere model, *Met O 20 DCTN 1*, Meteorol. Office, Bracknell, England, 1984.

Hansen, J., A. Lacis, D. Rind, G. Russell, P. Stone, I. Fung, R. Ruedy, and J. Lerner, Climate sensitivity and analysis of feedback mechanisms, in *Climate Processes and Climate Sensitivity*, *Geophys. Monogr. Ser.*, vol. 29, edited by J. Hansen and T. Takahashi, pp. 130–163, AGU, Washington, D.C., 1984.

Hibler, W. D., The role of sea ice dynamics in modelling $CO_2$ increases, in *Climate Processes and Climate Sensitivity*, *Geophys. Monogr.*

*Ser.*, vol. 29, edited by J. Hansen and T. Takahashi, pp. 238–253, AGU, Washington, D.C., 1984.

Jaeger, L., Monatskarten des Niederschlags fuer die Ganze Erde, Ber. Dtsch. Wetterdienstes, *18*, no. 139, 1976.

London, J., A study of the atmospheric heat balance, Final Report, AFCRC Contract AF19(122)-165, 99 pp., New York Univ., *DDC AD 117227*, New York, 1957.

Lyne, W. H., and P. R. Rowntree, Development of a convective parametrization using GATE data, *Met O 20 Tech. Note II/70*, Meteorol. Office, Bracknell, England, 1976.

Manabe, S., Climate and the ocean circulation, I, The atmospheric circulation and the hydrology of the Earth's surface. *Mon. Weather Rev.*, *97*, 739–774, 1969.

Manabe, S., and K. Bryan, $CO_2$-induced change in a coupled ocean-atmosphere model and its paleoclimatic implications, *J. Geophys. Res.*, *90*, 11,689–11,707, 1985.

Manabe, S., and R. T. Wetherald, Reduction in summer soil wetness induced by an increase in atmospheric carbon dioxide, *Science*, *232*, 626–628, 1986.

Manabe, S., R. T. Wetherald, and R. J. Stouffer, Summer dryness due to an increase of atmospheric $CO_2$ concentration, *Clim. Change*, *3*, 347–386, 1981.

Maykut, G. A., and N. Untersteiner, Some results from a time-dependent thermodynamic model of sea-ice, *J. Geophys. Res.*, *76*, 1550–1575, 1971.

Meehl, G. A., and W. M. Washington, Sea surface temperatures computed by a simple ocean mixed layer coupled to an atmospheric GCM, *J. Phys. Oceanogr.*, *15*, 92–104, 1985.

Mitchell, J. F. B., The seasonal response of a general circulation model to changes in $CO_2$ and sea surface temperature, *Q. J. R. Meteorol. Soc.*, *109*, 113–152, 1983.

Mitchell, J. F. B. On changes in soil moisture in $CO_2$ climate studies, *ESA SP-248*, pp. 171–173, Eur. Space Agency, Paris, France, 1986.

Mitchell, J. F. B., and T. S. Hills, Sea-ice and the Antarctic winter circulation: A numerical experiment, *Q. J. R. Meteorol. Soc.*, *112*, 953–969, 1986.

Mitchell, J. F. B., and G. Lupton, A $4 \times CO_2$ experiment with prescribed changes in sea temperatures, *Prog. Biometeorol.*, *3*, 353–374, 1984.

Mitchell, J. F. B., C. A. Wilson, and C. M. Price, On the specification of surface fluxes in coupled atmosphere ocean general circulation models, in *Coupled Ocean–Atmosphere Models, Elsevier Oceanogr. Ser.*, vol. 40, edited by J. C. J. Nihoul, pp. 249–262, Elsevier North-Holland, New York, 1985.

Mitchell, J. F. B., C. A. Wilson, and W. M. Cunnington, On $CO_2$ and clouds: Mechanisms of cloud changes due to tropospheric warmings, in *Numerical studies of the effect of increased atmospheric carbon dioxide on and climate*, Final report, CEC contract CL-114-UK(H), Meteorol. Office, Bracknell, England, 1986.

Mitchell, J. F. B., C. A. Wilson, and W. M. Cunnington, $CO_2$ climate sensitivity and model dependence of results, *Q. J. R. Meteorol. Soc.*, *193*, 293–322, 1987.

Palmer, T. N., and D. A. Mansfield, Wintertime circulation anomalies during past El Nino events, using a High Resolution General Circulation Model, I, Influence of model climatology, *Q. J. R. Meteorol. Soc.*, *112*, 613–638, 1986.

Reed, D. N., Simulation of time series of temperature and precipitation over eastern England by an atmospheric general circulation model, *J. Climatol.*, *6*, 233–253, 1986.

Reichle, D. E., J. R. Trabalka, and A. M. Solomon, Approaches to studying the global carbon cycle, Atmospheric carbon dioxide and the global carbon cycle. edited by Trabalka, J. R. *Rep. DOE/ER-0239*, pp. 15–24, U.S. Dep. of Energy, Washington D.C., 1985.

Richards, P. J. R., An objective assessment of specifications of boundary-layer eddy diffusion coefficients, *Met O 20 Tech. Note II/140*, Meteorol. Office, Bracknell, England, 1980a.

Richards, P. J. R., The parametrization of boundary layer processes in general circulation models, Ph.D. thesis, Univ. of Reading, England, 1980b.

Robock, A., The seasonal cycle of snow cover, sea-ice and surface albedo, *Mon. Weather Rev.*, *108*, 267–285, 1980.

Rowntree, P. R., Sensitivity of global simulations to the evaporation of convective condensates, *Met O 20 Tech. Note II/226*, Meteorol. Office, Bracknell, England, 1984.

Sasamori, T., J. London, and D. V. Hoyt, Radiation budget of the southern hemisphere, *Meteorol. Monogr.*, *13*, 9–23, 1972.

Schlesinger, M. E., and J. F. B. Mitchell, Model projections of equilibrium climatic response to increased $CO_2$ concentration, Projecting the climatic effects of increasing carbon dioxide, edited by M. C. MacCracken and F. M. Luther, *Rep. DOE/ER-0237*, pp. 81–148, U.S. Dep. of Energy, Washington, D.C., 1985.

Slingo, J. M., A cloud parametrization scheme derived from GATE data for use with a numerical model, *Q. J. R. Meteorol. Soc.*, *106*, 747–770, 1980.

Slingo, A (Ed.), Handbook of the Meteorological Office 11-layer Atmospheric General Circulation Model, *Met O 20 DCTN 29*, Meteorol. Office, Bracknell, England, 1985.

Slingo, A., and D. W. Pearson, A comparison of the impact of envelope orography and of a parametrization of orographic gravity-wave drag on model simulations, *Q. J. R. Meteorol. Soc.*, *113*, 847–871, 1987.

Slingo, A., and R. C. Wilderspin, Development of a revised long wave radiation scheme for an atmospheric general circulation model, *Q. J. R. Meteorol. Soc.*, *112*, 371–386, 1986.

Smith, R. N. B., An integrated approach to the representations of cloud processes, *Met O 20 DCTN 23.*, Meteorol. Office, Bracknell, England, 1985.

Somerville, R. C. J., and L. A. Remer, Cloud optical thickness feedbacks in the $CO_2$ climate problem, *J. Geophys. Res.*, *89*, 9668–9672, 1984.

Spelman, M. J., and S. Manabe, Influence of oceanic heat transport upon the sensitivity of a model climate, *J. Geophys. Res.*, *89*, 571 586, 1984.

Stephens, G. L., G. G. Campbell, and T. H. Vonder Haar, Earth radiation budgets, *J. Geophys. Res.*, *86*, 9739–9760, 1981.

Trabalka, J. R., J. A. Edmonds, J. M. Reilly, R. H. Gardner, and L. D. Voorhees, Human alterations of the global carbon cycle and the projected future, Atmospheric carbon dioxide and the global carbon cycle, *Rep. DOE/ER-0239*, pp. 247–287, U.S. Dep of Energy, Washington, D.C., 1985.

Washington, W. M., and G. A. Meehl, Seasonal cycle experiment on the climate sensitivity due to a doubling of $CO_2$ with an atmospheric general circulation model coupled to a simple mixed layer ocean model, *J. Geophys. Res.*, *89*, 9475–9503, 1984.

Washington, W. M., and G. A. Meehl, General circulation model $CO_2$ sensitivity experiments: Snow-sea ice albedo parameterizations and globally averaged surface air temperature, *Clim. Change*, *8*, 231–241, 1986.

Wetherald, R. T., and S. Manabe, An investigation of cloud cover change in in response to thermal forcing, *Clim. Change*, *8*, 5–24, 1986.

Wilson, M. F., and A. Henderson-Sellers, A global archive of land cover and soils data for use in general circulation climate models, *J. Climatol.*, *5*, 119–143, 1985.

Wilson, C. A., and J. F. B. Mitchell, Diurnal variation and cloud in a general circulation model, *Q. J. R. Meteorol. Soc.*, *112*, 347–369, 1986.

J. F. B. Mitchell and C. A. Wilson, Meteorological Office, Met O 20 Room 304E, London Road, Bracknell, Berks RG12 2SZ, England.

(Received January 26, 1987;
revised July 31, 1987;
accepted August 4, 1987.)